SEDIMENTOLOGY the journal of the International Association of Sedimentologists

Sedimentology (2014) **61**, 996–1030 doi: 10.1111/sed.12083

Two-layer scree/snow-avalanche triggered by rockfall (Eastern Alps): Significance for sedimentology of scree slopes

DIETHARD SANDERS, LUKAS WIDERA and MARC OSTERMANN
Institute of Geology and Palaeontology, University of Innsbruck, Innrain 52, A-6020 Innsbruck, Austria (E-mail: Diethard.G.Sanders@uibk.ac.at)

Associate Editor – Jaco Baas

ABSTRACT

Rockfalls that trigger scree-laden snow avalanches are common in mountain ranges, but the resulting avalanche development and its role in understanding the sedimentology of scree slopes are rarely described in detail. On Riepenwand (2774 m above sea-level, Kalkkögel range, Alps), on 6 May 2011 a 5800 m^3 rockfall of dolostone detached from the flank of a gorge in the upper part of the mountain. After first collapsing into the gorge, the fragmented rock mass fell down freely for 150 m onto a talus covered by coarse-granular snow. Rockfall impact triggered a medium-scale avalanche that developed: (i) a lower layer A of entrained, pure snow; and (ii) an upper layer B of clay-sized to boulder-sized fragments mixed with snow. This 'two-layer scree/snow avalanche' halted in the distal slope segment of the talus. Boulders within layer B mainly came to rest in the distal part of the avalanche deposit. Fragments smaller than cobble-size grade did not show obvious downslope segregation. With snowmelt, the rockfall fragments dispersed in layer B were concentrated to a clast-supported veneer that was draped over the older talus surface upon slower melting of avalanche layer A. In the grain-size fraction ≤16 mm, a mean of 5 wt% matrix (silt-sized to clay-sized grains) of the rockfall-derived scree of layer B is similar to a mean matrix content of 7 wt% within stratified talus slopes of the Kalkkögel range. This similarity suggests that a major share of matrix – widespread in stratified talus – stems from rockfalls. The characteristics of the scree veneer as melt-lag of a scree-laden snow avalanche will be blurred with time. Fossil talus successions may contain a substantial proportion of scree carried down by snow avalanches. The formation of a distinct sedimentary facies of snow avalanche-deposited scree is impeded by processes of redeposition and deposit modification on talus.

Keywords Alps, matrix, rockfall, scree slope, snow avalanche.

INTRODUCTION

Effects of snow avalanches on the shape and surface characteristics of scree slopes are described in many papers, chiefly with a geomorphological perspective (e.g. Rapp, 1959, 1960; Gardner, 1970; Luckman, 1977, 1988; Corner, 1980; Fitzharris & Owen, 1984; Ward, 1985; Ballantyne, 1987; André, 1990; Bell *et al.*, 1990; Jomelli & Francou, 2000; Jomelli & Bertran, 2001; De Scally & Owens, 2005; Decaulne & Saemundsson, 2006, 2010; Owen *et al.*,

Dedicated to the memory of our colleague Lorenz Keim, PhD, who died in a snow avalanche on 4 February 2012.

2006; Johnson & Smith, 2010). Most examples of scree transport by snow avalanches were interpreted weeks to months after the event, when the deposit had already been modified by snowmelt; this is explained by the sheer remoteness of many sites and/or the danger of access during winter to spring. In addition, the precise timing of snow avalanching at a given site, and the type of avalanche formed, are difficult to foresee. Scree-laden snow avalanches triggered by large rockfalls hence are rarely, if ever, described immediately after occurrence.

Although snow avalanches are common on talus slopes, to date only a few authors have suggested criteria for identification of avalanche-deposited scree (Blikra & Nemec, 1998; Blikra & Selvik, 1998; Nemec & Kazanci, 1999). A distinction between surface features of scree slopes and sedimentary facies of talus is significant because only a limited set of process indicators – as seen on the surface – can enter the final sedimentary record. As outlined herein, snow-avalanche transported scree perhaps comprises a significant proportion of talus successions, yet clear-cut distinction from other processes of transport and depositional overprint may remain difficult. Another question in talus sedimentology which is still largely unsolved concerns the origins of matrix of silt-size to clay-size grade. In the field, this matrix appears as a more-or-less cohesive mud. Apart from clasts mainly of pebble to boulder size, talus successions invariably host a substantial amount of matrix (Sanders *et al.*, 2010). This was cursorily noted previously (e.g. Ampferer, 1907; Rapp, 1960; Brückl *et al.*, 1974; Luckman, 1977; Ballantyne, 1987; Hinchliffe *et al.*, 1998; Bertran & Texier, 1999; Curry & Morris, 2004) but was not taken as a separate research focus. First results from carbonate-lithic scree slopes of the Eastern Alps indicated that matrix can result from variegated processes acting both on the rock cliffs and on the talus (Sanders *et al.*, 2010). Depending on volume and fall height, rockfalls generate more-or-less large dust clouds that may veneer extensive areas after fallout (cf. Wieczorek *et al.*, 2000; Sanders *et al.*, 2010; Heckmann *et al.*, 2012). Rockfall-generated dust, however, is investigated only rarely in itself (Wieczorek *et al.*, 2000), and the potential role of rockfalls in contributing matrix to scree-slope successions as yet is poorly documented.

This article describes transport, deposition and modification of scree in a wet-snow avalanche forced off by a rockfall *ca* 5800 m^3 in volume that happened on 6 May 2011. The avalanche developed into a two-layer snow flow consisting of: (i) a layer of pure avalanche snow gathered by entrainment; overridden by (ii) a layer of rockfall-derived scree (boulders to clay-size grade) mixed with snow. The rockfall took place in the Kalkkögel range near the doorstep of Innsbruck city (Austria; Fig. 1), was recorded seismographically, and was photographed a few hours after the event from a helicopter. In addition, the deposit could be reached easily by hiking a 900 m ascent. Together, these factors provided a rare opportunity to document: (i) a scree-laden snow avalanche practically since the moment of deposition; (ii) the characteristics and distribution of clastic material in the pristine avalanche deposit; (iii) modification of deposit characteristics during snowmelt; and (iv) the contents and grain-size distribution of rockfall-generated matrix within the upper avalanche layer. The observations presented herein imply that a significant proportion of the matrix of scree slopes may originate during larger rockfalls.

SETTING

Geology

The Kalkkögel range (Fig. 1) is part of the Eastern-Alpine (Austroalpine) edifice that consists of stacked thrust nappes derived from the northern margin of the Apulian microcontinent (Schmid *et al.*, 2004). The range consists of a Triassic metasedimentary series resting parautochthonous on polymetamorphic Austroalpine basement (Geyssant, 1973; Frank *et al.*, 1987). With respect to morphology, the range is dominated by two thick successions of metadolostones that originally accumulated in peritidal environments of carbonate platforms (Geyssant, 1973; Brandner *et al.*, 2003). During Early Cretaceous orogenic nappe stacking, the future Kalkkögel were overridden by structurally higher nappes, and metamorphosed at *ca* 450°C and 3·5 to 4 MPa (Dietrich, 1983; Donofrio, 2008). In the Triassic platform dolostone series, metamorphism was not associated with penetrative shearing and dynamic recrystallization; as a result, both bedding and a few of the original sedimentary structures (for example, tepees and beds with stromatolithic lamination) are still identifiable. The basal part of the Triassic series had cooled to less than *ca* 110°C (apatite fission-

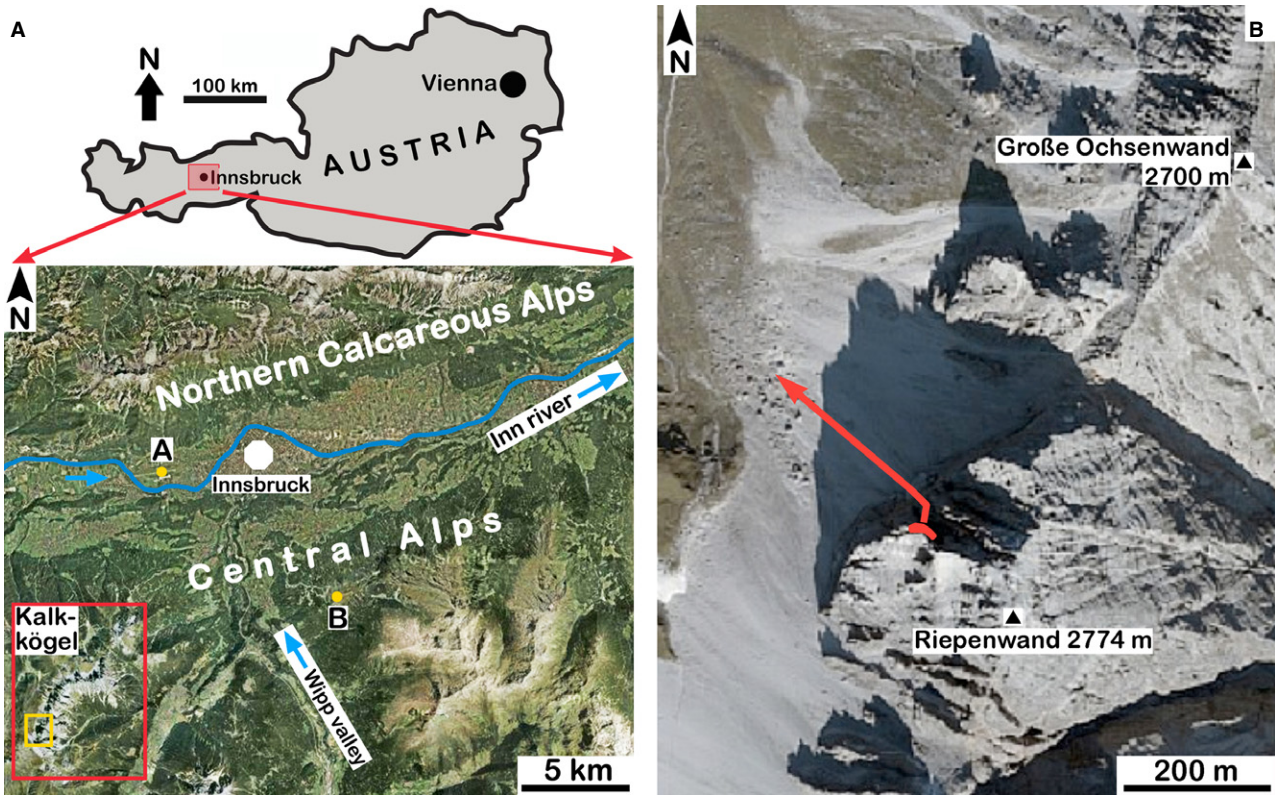

Fig. 1. (A) Position of the Kalkkögel range in Austria. Yellow rectangle shows area in panel (B). 'A': Meteorological station Innsbruck-Flughafen (579 m a.s.l.); 'B': meteorological station Patscherkofel (2247 m a.s.l.). (B) Mount Riepenwand, with detachment area of rockfall of 6 May 2011 (red blotch) and approximate downslope trajectory of rockfall material (red arrow).

track closure) at *ca* 60 Ma (Fügenschuh *et al.*, 1997, 2000). At many locations, the metasedimentary succession abuts the underlying basement along normal faults of large throw (Brandner *et al.*, 2003). These faults result from extension and lateral escape at right angles to the compression exerted by the South-Alpine indenter (Fügenschuh *et al.*, 2000). Global positioning system data and fault-plane solutions of earthquakes along Wipp valley and Inn valley (cf. Fig. 1) indicate that structural shortening persists, or became re-activated (Reiter *et al.*, 2005).

The central and southern parts of the Kalkkögel range, including Mount Riepenwand, consist of Upper Triassic metadolostones (Hauptdolomit unit, Norian) up to 800 to 850 m in thickness (Fig. 1B; Brandner *et al.*, 2003). As a result of subhorizontal to low-dipping, very thick bedding of the Hauptdolomit, summits tend to be of castellate form (cf. Cruden & Hu, 1999). During the Last Glacial Maximum (LGM), the peaks of the Kalkkögel higher than 2300 to 2400 m a.s.l. stood as nunataks above the reconstructed ice surface (Van Husen, 1987). The scree slopes along the western face of the Kalkkögel range downlap onto glacigenic deposits comprising terminal and lateral moraines, 'fluted' moraine and rock glaciers (cf. Ladurner, 1932; Ampferer, 1943; Fig. 1B). The chronostratigraphy of the glacigenic succession to date is not established. Comparison with age-dated late-

Fig. 2. (A) Satellite image of the north-western part of Riepenwand, with 'summit gorges' debouching into a subvertical cliff. Rockfall volume of 6 May 2011 ('6511') is indicated by a red-shaded area. The scree slope is herein subdivided into sectors I to V (see Table 1). The 6511-rockfall mainly affected sector III. Letters 'A' to 'K': Pre-6511 rockfall boulders used as local reference system. (B) Laser scan of area in (A), showing the extent of rockfall-induced avalanche, and approximate area of 'splash haloes' of rockfall impact. Inset in lower right: 2 m-isohypse LIDAR-based profile along the summit gorge, cliff and scree slope. No vertical exaggeration. Alpha: Shadow angle, 30°; beta: fahrböschung, 54° (see text for discussion). Maps for both panels from: http://tiris.tirol.gv.at/.

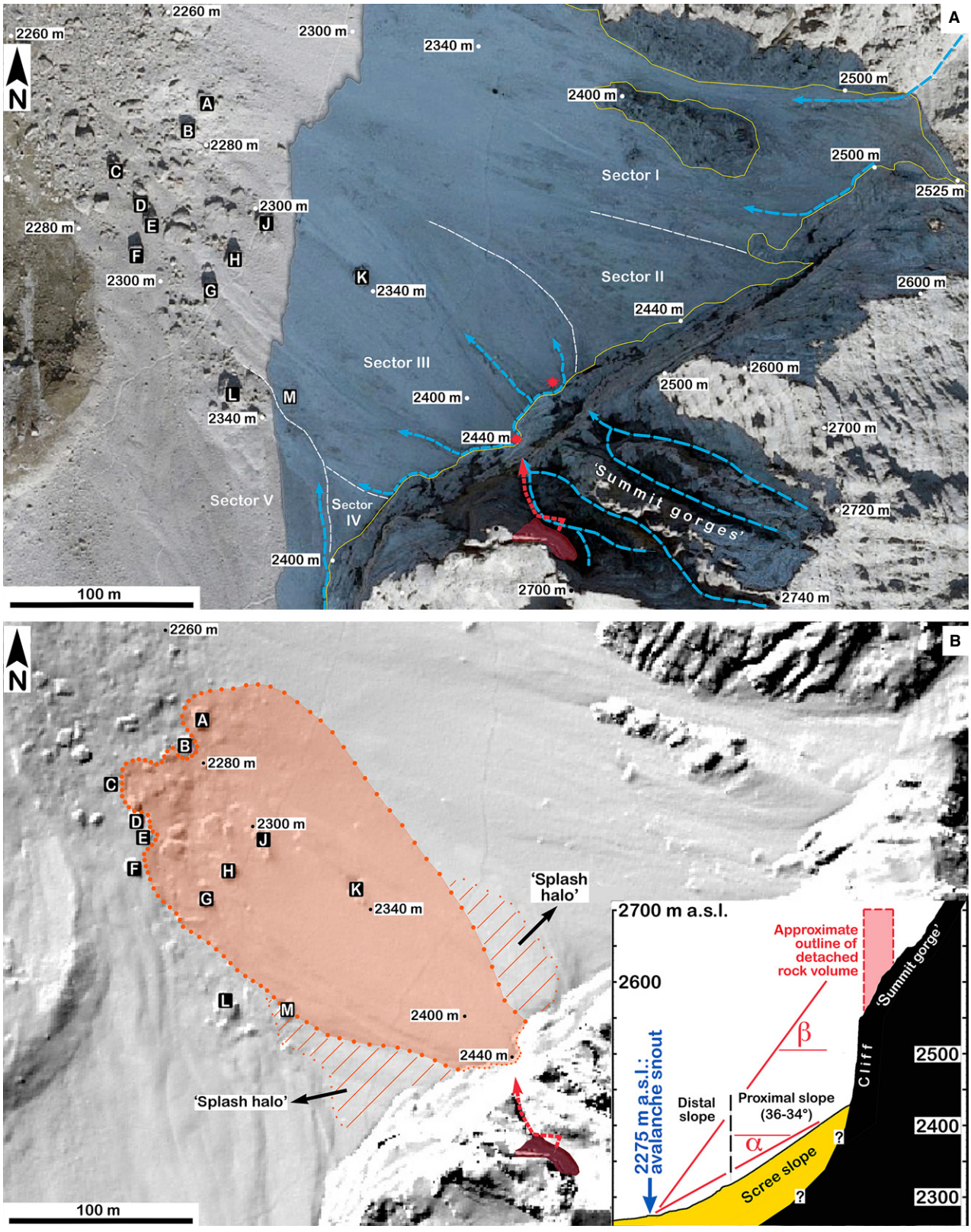
A
N
2260 m
2300 m
2340 m
2500 m
2400 m
2280 m
2500 m
2525 m
Sector I
2300 m
2280 m
2300 m
Sector II
2600 m
2340 m
2440 m
Sector III
2600 m
2500 m
2400 m
2340 m
2700 m
2440 m
'Summit gorges'
Sector V
Sector IV
2720 m
2400 m
2700 m
2740 m
100 m
B
N
2260 m
2280 m
2300 m
2340 m
'Splash halo'
2400 m
2440 m
'Splash halo'
100 m
2700 m a.s.l.
Approximate outline of detached rock volume
2600
'Summit gorge'
β
Cliff
2500
Distal slope
Proximal slope (36-34°)
2275 m a.s.l.: avalanche snout
α
2400
Scree slope
?
?
2300

glacial moraines near the area, however, suggests that the glacigenic package along the western face of Kalkkögel accumulated mainly during the Daun to Kromer–Kartell stadials (terminal part of the late-glacial to early Holocene; cf. Kerschner, 1986; Ivy-Ochs *et al.*, 2006, 2009).

Mount Riepenwand and talus

Mount Riepenwand consists of a lower edifice bounded by vertical cliffs between *ca* 150 m and 300 m in height, depending on location, and a roughly pyramid-shaped upper edifice up to the summit (Fig. 1B). The north-west facing facet of the upper edifice is riddled by deep 'summit gorges' that formed by incision along a prominent set of structural discontinuities (joints and faults; Figs 2A and 3; Sanders, 2011). Snow trapped in the gorges turns to corn snow later in the year, but no perennial tongues of ice or firn are known. The summit gorges are conduits for rockfalls detached from their flanking cliffs, and for surface runoff (Fig. 3).

The north-west facing scree slope of Riepenwand, herein termed Riepen talus, is divided into five sectors (Table 1; Fig. 2A). On slope sectors I and II small, full-depth wet-snow avalanches probably triggered by instability of the snow cover are common. Conversely, on slope sector III, of most interest herein, snow avalanches were not observed prior to the considered rockfall. In its distal, low-dipping part (*ca* 2260 to 2300 m a.s.l.) the surface of slope sector III consists of boulders to fine pebbles (Figs 2 and 3). Cursory field observations since 2001, and comparison with satellite images from 2000 to 2007 (www.tirol.gv.at/statistik-budget/statistik-tiris/tiris-kartendienste/), indicate that the distal part of sector III is rarely supplied with sediment; this is also supported by fully lichenized surfaces of pebbles to boulders. Upslope of 2300 to 2305 m a.s.l., prior to the 6511-rockfall, the surface of slope sector III consisted of cobbly to pebbly scree, and showed an overall upslope fining of mean grain size (Fig. 3). Upward of 2320 m a.s.l.,

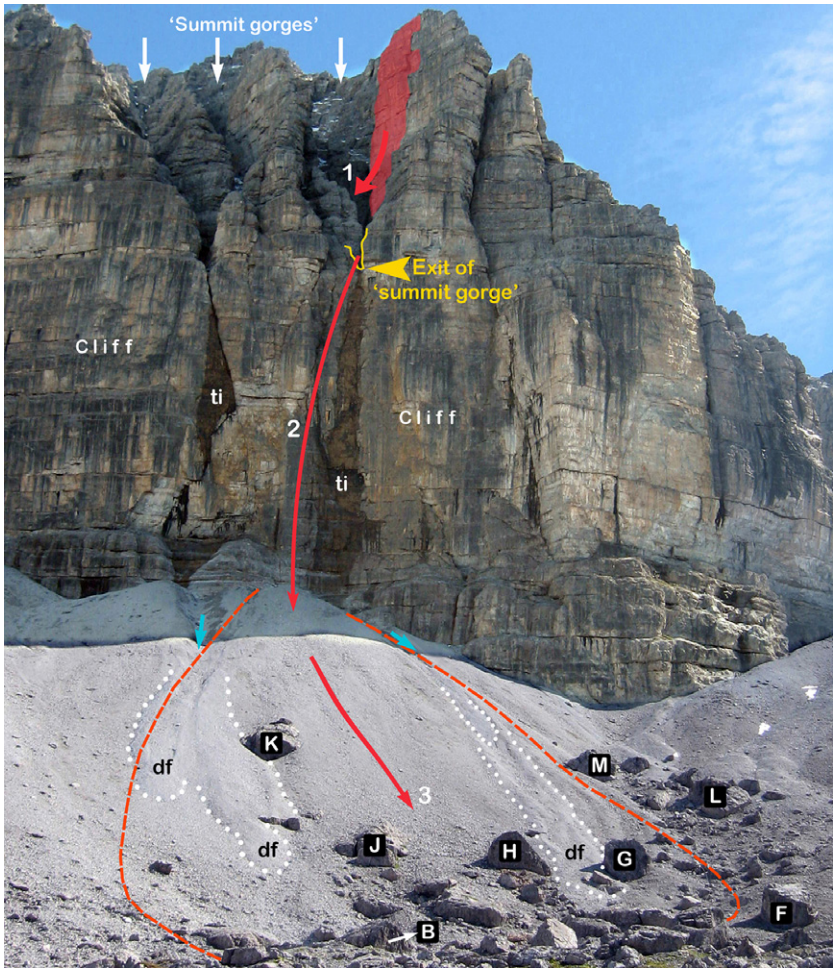

Fig. 3. North-west face of Riepenwand, with scheme of rockfall/snow-avalanche. Photograph taken prior to the event. The summit gorges (white arrows) focus surface run-off and rockfalls detached from their flanks. The cliff bears two tintenstriche (ti) that are wet for most of the year. The exit of the summit gorges corresponds with two incised chutes (blue arrows) on the scree slope. The chutes conduit ephemeral surface run-off and debris flows (df). The red-shaded area shows reconstructed fallen rock volume. The rock mass collapsed into the summit gorge (1) and fell down freely over *ca* 150 m in height onto the snow-covered talus (2; see also Fig. 5). The impact of the mass of rock fragments triggered an avalanche composed of scree and snow (3, see text). Dashed red line: approximate outline of the 6511-avalanche deposit (cf. Fig. 5). Pre-6511 rockfall boulders labelled 'B' to 'K' provided a local reference system (Fig. 2).

Table 1. Features of scree-slope sectors I to V along Riepenwand (see Fig. 2).

Slope sector	Supply, characteristics	Remarks
Sector I	Supplied by rockfalls from Riepenwand and from the southern pedestal of Grosse Ochsenwand (cf. Fig. 1B). Lower part of slope of concave shape, merges laterally with sector II	On both slope sectors I and II, small, full-depth avalanches are common in spring (based on 11 years of observation) Downslope redeposition of scree mainly by particle creep, frictional grain flow, and transport by full-depth snow avalanches
Sector II	Supplied by rockfalls from Riepenwand. Lower part of slope of concave shape, merges laterally with sector I	
Sector III	Supplied by rockfalls focussed mainly into the summit gorges of Riepenwand cliff, resulting in point input of scree. Dull-cone shaped apical part of relatively well-sorted, fine-grained composition. Distal part of slope with boulders	No full-depth snow avalanche was observed on this part of the slope before the rockfall event of 6 May 2011
Sector IV	Cliff above this slope sector is 220 m in height. Slope sector supplied by: (i) small rockfalls and wash-down of material from the rock cliff above; and (ii) in its distal part, from lateral advection of material from sectors III and V. Supply by small rockfalls and wash-down of material from the rock cliff produced a scree ridge *ca* 1 m in height along the cliff toe	Small slope sector of distinct character
Sector V	Supplied with scree from the west and south-west facing cliffs of Mount Riepenwand (see Fig. 1B) and from the north-west slope of Schlicker Seespitze (2804 m a.s.l., not shown)	Ground avalanches common: (i) avalanches detached within and riding on snow cover (= not relevant to scree transport); and (ii) full-depth avalanches with scree

prior to the rockfall, the talus surface steepened over a distance of a few tens of metres into a rectilinear proximal slope segment *ca* 170 m in length (inset profile in Fig. 2B). The small, but distinct slope sector IV is not influenced by linear surface run-off (Fig. 2A). The apex of this talus sector is a ridge about 1 m in height parallel to the cliff toe; such ridges are depositional features formed by small rock showers, 'wash-down' of material from the cliff surface during rain storms, and stone-laden snow cascading down (Kilian, 2008). Slope sector V is supplied with scree both from Riepenwand and from another summit further south (Schlicker Seespitze, 2804 m a.s.l.; not shown). There are no quantitative data on the thickness of corn-snow cover on slope sector III immediately before the rockfall event on 6 May 2011 (in the following briefly designated as 6511-event). On 11 May 2011, the first field trip to the location, the snow cover on the well-lit moraine field ahead of the western cliffs was patchy, but attained more than 1 m in thickness in morphological depressions. It is thus inferred that the snow cover on Riepen talus was at least a few decimetres to one metre in thickness on the day of the event.

Climate

No temperature and precipitation records are available for the Kalkkögel range. The two nearest meteorological stations are Patscherkofel (2247 m a.s.l.) and Innsbruck-Flughafen (579 m a.s.l.; Fig. 1A). Their records, and contoured maps of monthly climate relative to the mean of 1971 to 2000 (available at www.zamg.at), indicate that late winter and spring 2011 had been exceptionally warm and dry (Fig. 4A and B). In the monthly means, an above 'mean 1971 to 2000' precipitation is indicated for May 2011 (Fig. 4B). From 1 May to 4 May 2011, in the

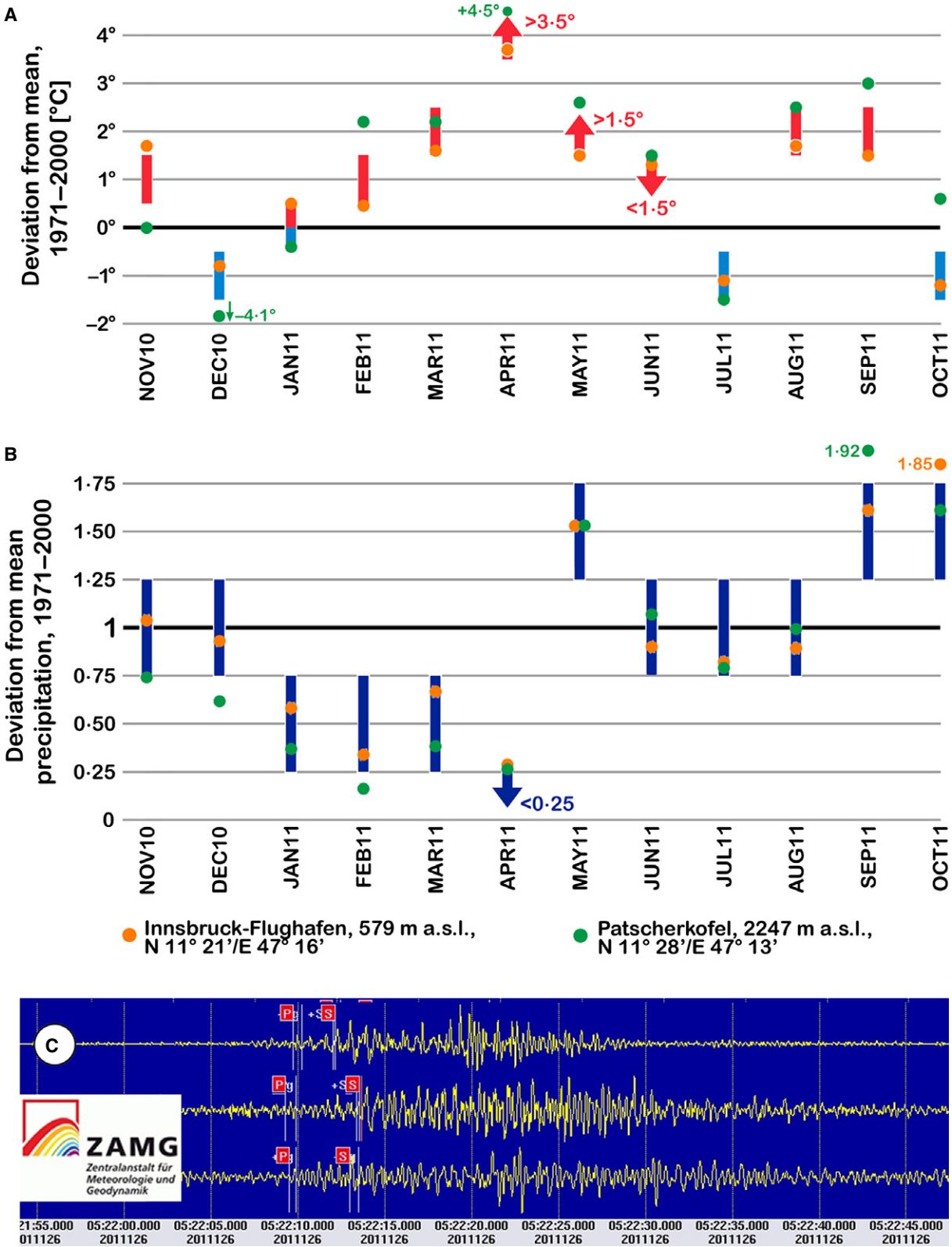

Fig. 4. Temperature (A) and precipitation records (B) of meteostations near the Kalkkögel range. Dots indicate monthly means for station Innsbruck-Flughafen and station Patscherkofel (see Fig. 1A). Red and blue bars are taken from contoured monthly climate maps. (C) Seismograms of three locations nearest to the rockfall event. Data source for (A) to (C): Zentralanstalt für Meteorologie und Geodynamik, Vienna (www.zamg.ac.at/fix/klima/jb2011/index_e.html).

region of Innsbruck, temperatures above the 1971 to 2000 mean were combined with cloudy sky but only trace amounts of rain; fair weather re-established on 5 May. The higher than average mean monthly precipitation of May 2011 (Fig. 4B) was attained almost entirely during the second half of the month. There is thus no evidence that the 6511-rockfall was triggered by strong precipitation. The potential role of the exceptionally warm late winter and spring is discussed below.

Seismic activity

There is no evidence that the rockfall of 6 May 2011 was triggered by a macroseismic event. According to the seismic record of the Zentralanstalt für Meteorologie und Geodynamik (Vienna), for May 2011, an event with an epicentral Richter magnitude $M = 2{\cdot}3$ took place on 13 May in Gurk, approximately 250 km ESE of Riepenwand. In addition, two stronger earthquakes at remote locations (a: Murcia region, Spain, $M = 5{\cdot}1$, 11 May; b: western Turkey, $M = 5{\cdot}8$, 19 May) were not macroseismically recorded in the study area, and not of correct timing to provide an explanation for the 6511-event (see: zamg.ac.at/fix/geophys/K11-05.pdf). On 21 June 2011, another notable rockfall took place on Riepenwand, albeit much smaller in volume than the event of 6 May (see below). Again, there is no evidence that the second rockfall was triggered by macroseismicity: at 00:14 hours on 22 June 2011 an earthquake of $M = 2{\cdot}9$ epicentred near the village of Axams, 7 km north of Riepenwand, *ca* 8 h after the rockfall of the preceding day (see: zamg.ac.at/fix/geophys/K11-06.pdf). There is also no report of another larger rockfall from Riepenwand that could have been triggered by that earthquake.

METHODS AND DEFINITIONS

Snow shows an extremely wide range of physical properties, as does the behaviour of avalanches (e.g. Pudasaini & Hutter, 2007). In the present study, if not otherwise noted, only ground-hugging avalanches (ground avalanches) are addressed, because this is the avalanche type of the considered event. The term 'scree' is herein used as an umbrella for all talus material of boulder-size to clay-size grade. Because investigations of Riepen talus had started earlier (Kilian, 2008; Reichhalter, 2009), both the scree slope and the cliff were photographed every year since spring 2008. These investigations facilitated identification of changes due to the 6511-rockfall. Comparison of field photographs of the rockfall detachment area before and after the event, and comparison of field photographs with satellite orthoimages and LIDAR-based topography taken before the event, allowed the outline of the detached rock mass within a LIDAR-based, three-dimensional isohypse model with 2 m altitude resolution. Volume determination was made in AutoCAD (Version 2009) by addition of the volumes of 2 m altitude increments of the defaced rock mass (Fuhrmann, 2012). The characteristics and changes of the 6511-deposit were inspected during a total of eight field trips from 11 May (first) to 5 October (last) in the year 2011, and by three field trips in 2012 (last on 3 October 2012). Until September 2011, due to frequent smaller scale rockfalls, it was impossible to approach the apex of Riepen talus. In the field, to distinguish older scree from material brought down with the 6511-event and its aftermath, a distinct difference in degree of weathering, infestation and lichenization of rock surfaces was taken as an indicator. Boulders scattered on the talus surface before the event were spotted and labelled in satellite orthophotographs, in LIDAR images, and in the field (cf. Figs 2 and 3). Boulder labelling was done to: (i) clearly identify new boulders brought in by the 6511-event; and (ii) help in mapping the extent of the 6511-deposit. Field mapping of the deposit was done in comparison with pre-rockfall laser scans and satellite orthophotographs.

To document the grain-size distribution of the sediment fraction smaller than 16 mm grain size, 11 samples each *ca* 2·5 to 3 kg were collected. To achieve a representative grain-size distribution of the *entire* 6511-event deposit, because of the abundance of cobbles to boulders, at least a few tons of sediment including boulders should be sieved (see, e.g. Crosta *et al.*, 2007). To determine the content of clay-sized to sand-sized material in the sediment fraction up to 16 mm, however, samples of the indicated mass were sufficient. The scree veneer on top of the 6511-avalanche was sampled in the distal part of the deposit, i.e. in the part that had been accessible since the day of the rockfall event. Sampling locations were distributed randomly across the distal part of the avalanche deposit. At each location, the scree veneer of typically some 10 to 30 cm in thickness (see below) was

Fig. 5. (A) Riepenwand, 6 May 2011, 12:13 hours. Note the elongate shape of the scree/snow avalanche deposit (upper part outlined by white dots). Abundant smaller rockfall still fell out of the summit gorge (cf. Figs 2 and 3). Note the outer limit (red dots) of rockfall dust settled on snow. (B) Rockfall-induced avalanche, 6 May 2011, 12:13 hours. Pre-rockfall boulders are labelled 'B' to 'M' (see Fig. 2). Note the elongate shape and marginal rim of the avalanche deposit. Boulder cluster labelled 1 (red arrow) and boulder labelled 2 (red arrow) were deposited during the event. (C) Detail of (B). Cluster of 6511-rockfall boulders (labelled 1) in the proximal part of the slope. Red dots mark the boundary between avalanche and splash halo of pebble to clay-sized material blown out upon rockfall impact. Note also the track of a 'latecomer boulder' (red arrows) rolled down on top of snow cover. (D) Detail of (B). Note: (i) margin and front of 6511-avalanche; (ii) 6511-boulder labelled 2; and (iii) track of 'latecomer boulder' rolled down on the avalanche deposit (red arrow). Photographs (A) to (D) by Dr Michael Said. (E) Rockfall scar (outlined by red dots), and rockfall boulder pinched in the summit gorge, 6 May 2011, *ca* 14:00 hours. Photograph by Heinz Moser. (F) Rockfall on 21 June 2011. This event mainly resulted in a dust cloud, and did not affect the distal part of the 6511-deposit. Photograph available at: http://tirol.orf.at/stories/522404/.

sampled down to its base. Because only the grain-size distribution of the sediment fraction up to 16 mm was in target, larger pebbles to cobbles were not sampled in the field. On 16 September 2011, the frequency of rock falls was low enough for the first time to allow for sediment sampling of the apex of Riepen talus under sensible risk. At the apex, three samples were taken from the flank of a small ravine incised into the apical sediment (see illustrations below). As outlined below, the apical sediment sampled on 16 September 2011 is not identical to the apical sediment of the day of the rockfall event. Nevertheless, the apex was sampled for comparison with the scree veneer in the distal part of the avalanche deposit. The grain-size distributions up to 16 mm in size of the samples from the 6511-event deposit and of the talus apex were compared with the same sediment fraction (up to 16 mm in size) from stratified talus slopes of the Kalkkögel range. The stratified talus slopes were sampled per layer from surface to bottom within a total of 11 ditches excavated down to *ca* 50 to 60 cm below the slope surface. In the ditches, individual strata were distinguished by vertical differences in mean grain size and sorting. These strata were sampled in total, that is, no clast size fraction was omitted (as in the case of the 6511-sediment veneer in the distal part of the avalanche deposits). In the final assessments of grain-size distributions, however, only the relative weight percentage of grain size classes up to 16 mm was considered. All of the sediment samples were sieved by washing. Before sieving, each sample was dried for 24 h at 50°C in a stove, then weighed. The dry weighed sample then was bathed in water plus a few drops of rinsing agent, to prevent coagulation of fine-grained sediment. After 24 h of waterlogging, the samples were churned gently to disintegrate potential clumps of the mud-sized sediment fraction, then sieved. The sediment fractions between 4 mm and 0·063 mm in calibre were sieved under shaking with 50 Hz for 45 min. The sediment fraction <0·063 mm in grain size (silt-size to clay-size), mud-size fraction, was held back. Next, all grain-size fractions were dried at 70°C for at least 12 h, then weighed.

The grain-size distribution of the rockfall-produced sediment fraction smaller than 2 mm in size was determined with a Malvern Mastersizer 2000® laser diffractometer (Malvern Instruments Limited, Malvern, UK) with a size detection range from 0·02 to 2000 μm. In preparation for measurement, the samples were dry-sieved gently to eliminate particles >2 mm in size. Dry sieving was preferred to prevent, as far as possible, potential dissolution loss of ultra-fine particles. To prepare the solution for laser measurement, 25 g of Calgonit® (active constituent: sodium hexametaphosphate; $[NaPO_3]_6$) was dissolved in 500 ml of Aqua bidest. Next, 1 g of dry-sieved sample was stirred up in 5 ml of the solution, plus 5 ml of Aqua bidest. The resulting sample solution then was left to rest for *ca* 10 h, to enable discoagulation of aggregates of fine grains. In this step, part of the ultra-fine sediment fraction may have been lost by chemical dissolution (see below for discussion). Measurements were made with a red He-Ne laser (wave length 0·632 μm) and with blue light (wave length 0·466 μm). Each sample solution was measured 18 times, subdivided into packages of three measurements each (six packages in total). Each package was immediately preceded by an ultrasonic impulse 15 sec in duration, to disaggregate potential clumps of fine grains. *During* measurements, the duration of ultrasonic input was increased in 15 sec increments, from 0 sec in the first package to 90 sec in the final pack-

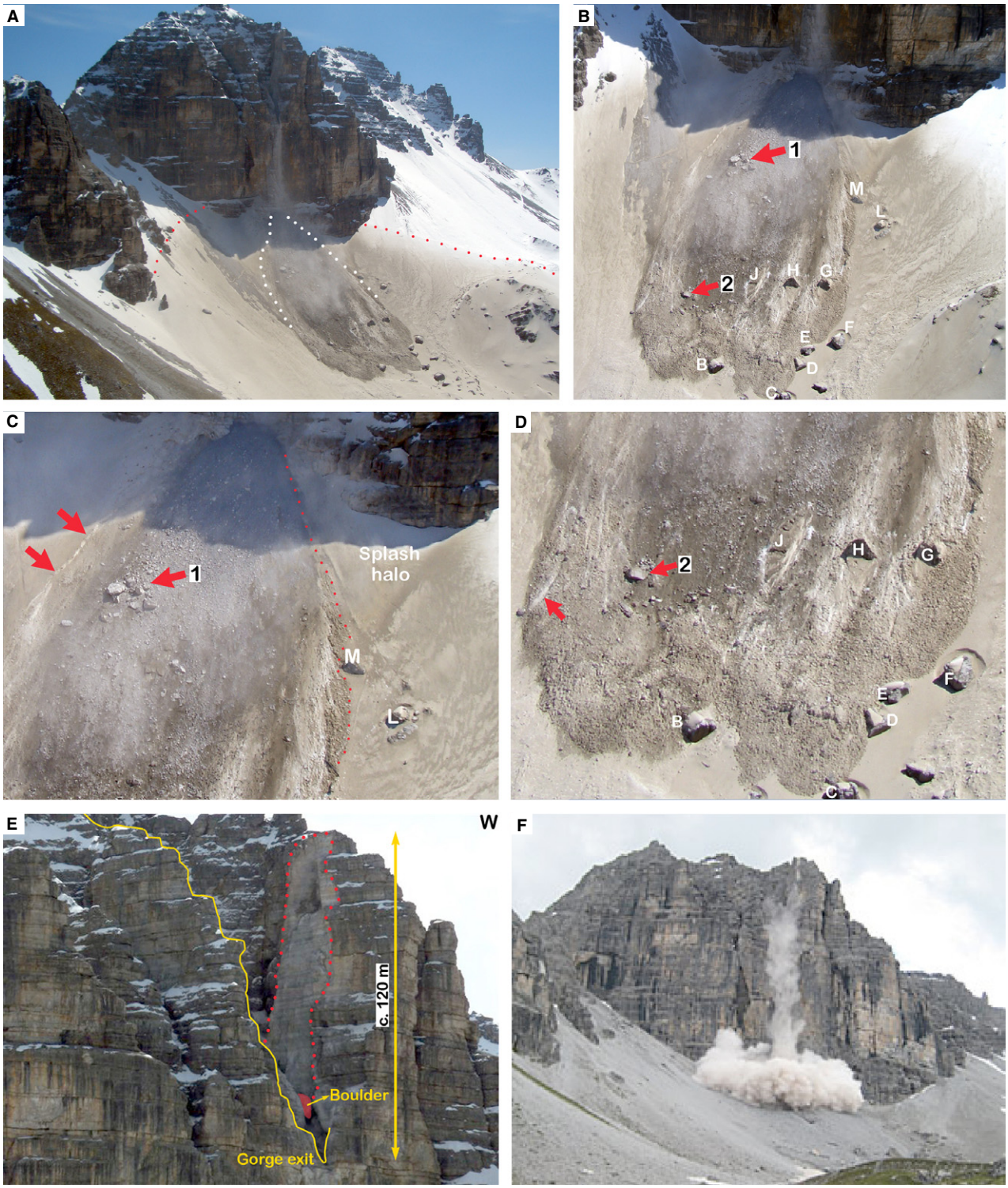

age. Automated calculation of grain-size distribution was based on Fraunhofer diffraction theory. Grain-size distributions were calculated with a mean refractive index of dolomite of 1·65, and an absorption coefficient AC of 0·1; in fine-grained carbonate deposits, this AC has proven sufficient to eliminate artificial peaks (see Sperazza *et al.*, 2004). A few samples were re-calculated with an AC of 0·5; the resulting grain-size distributions did not change with respect to their bimodal form, and only insignificantly with respect to relative volume per-

centages, from those calculated with AC = 0·1. This distribution supports the overall validity of results. The intensity of the diffracted laser light was detected with 52 sensors, and with 1000 detections per second.

Six samples were chosen for scanning electron microscope (SEM) investigation of the dust fallout and of fine-grained matrix generated during the rockfall event. For SEM inspection, a small portion of dry fine-grained sediment was littered onto a chip of adhesive tape, and inserted unsputtered into the SEM vacuum chamber. Electron microscopic inspection was done with a Digital Scanning Microscope JEOL JSM-5130LV (JEOL Limited, Tokyo, Japan) in low-vacuum mode, at 25 kV acceleration voltage, a gun current of 5 μA, with a backscattered electron detector. Scanning electron microscope inspection of angular, very fine-grained materials is cumbersome due to electric charging of edges and peaks, and trembling or jumping of grains; overall, however, the samples were stable enough to allow for photographs up to a magnification of 3·5 to 5 k.

THE ROCKFALL

Event on 6 May 2011

The rockfall, with a reconstructed total volume of 5878 m^3 (Fuhrmann, 2012), induced a microseismic event. The earliest P-wave incidence was recorded at 05:22:9·3 UTC (07:22:9·3 hours local time; Fig. 4C). From the first incidence of P-waves, the seismograms show an overall gradual increase in amplitude, in particular after the incidence of S-waves a few seconds later. Wave trains of relatively large amplitude persist until *ca* 07:22:30 to 07:22:40 local time, then gradually fade out to background (Fig. 4C). In the seismograms, the poor differentiation into wave packages combined with gradual fadeout of ground acceleration is considered typical of gravitational mass movements. No other microseismic event was recorded in this area for 6 May 2011, suggesting that the main event from collapse into the gorge via free fall over the cliff to stopping of the scree-laden snow avalanche needed between *ca* 20 sec and 30 sec.

The rockfall produced a large dust cloud that was not photographed. A constraint on cloud size, however, was deduced by dust fallen out onto snow and vegetation near the avalanche deposit (Fig. 5A). The dustfall indicated that the cloud had a size of *ca* 800 × 500 m, which is probably a minimum estimate. The dust fallout on snow was of overall northward-skewed shape, i.e. the cloud slowly drifted towards the north while settling. In the morning on 6 May 2011, the Tyrolean federal emergency centre received a telephone call indicating 'smoke' by the caller who reported a fire. Examination with binoculars, however, showed that it was dust, and it was assumed correctly that a larger rockfall had taken place. At that time of the year, the Kalkkögel range is only occasionally visited by hikers or back country skiers. Because fatalities were not expected, a search was not started immediately. A request to check the situation was, however, sent to an ambulance helicopter that was to set off to a ski resort on a glacier south-west of the Kalkkögel. Helicopter flight #342/2011 took off from Innsbruck airport at 12:08 hours, and passed Riepen talus between 12:13 hours and 12:14 hours. On this first pass, the area was photographed from the helicopter. On the occasion of the first helicopter bypass the extent and lobate shape of the mixed snow/scree avalanche was developed fully as observed on the first field trip (Fig. 5A to D). These observations suggest that the rockfall events that were responsible for shaping the final snow/scree deposit indeed had started at 07:22 hours local time.

When the helicopter first passed by, the large dust cloud of the main event had already settled. Smaller subsequent rockfalls, however, continued to produce dust veils (Fig. 5A). None of these subsequent rockfalls, however, was of sufficient volume to change the external shape and features of the entire deposit. In the upper part of the talus, however, numerous smaller rockfalls that continued for months after the main event led to vertical aggradation in the range of a few metres (see below). On the same day (6 May 2011), the next helicopter flight #343/2011 started at 13:33 hours from Innsbruck airport, and Riepen talus was passed again between 13:38 hours and 13:39 hours and photographed a second time. On this occasion, the mixed snow/scree avalanche showed the very same features as during the first pass. Smaller rockfalls and associated dust veils, however, continued with practically the same intensity as during the first bypass. Around 14:00 hours on 6 May, the rockfall deposit was seen from the ground by a hiker who was resting in front of Adolf-Pichler hut (1977 m a.s.l.). The hiker photographed the defacement scar of the rockfall

from *ca* 1 km distance (Fig. 5E) with a zoom lens. Closer examination was not possible due to perpetual rumbling and crashing of rockfalls. Comparison of these photographs and photographs taken five days later, further underscore that the major volume of rockfall took place in the morning on 6 May 2011.

Early aftermath

The first field trip was made five days after the event, on 11 May 2011. The defacement scar of the rockfall and the avalanche deposit were photographed, and samples of rockfall-generated dust and sediment were collected. On 11 May, small rockfalls still defaced nearly perpetually from the scar, and the proximal sector of Riepen talus was exposed to numerous impacts. Small rockfalls were reported to have taken place every day from the same defacement scar that had formed on 6 May in the vicinity of the Adolf-Pichler hut (which opened on 1 June 2011). Local information indicated that rockfall activity diminished overnight but then intensified during the late morning of the next day, concurring with later field observations.

On 21 June 2011, another notable rockfall occurred close to 16:00 hours. This event, too, was photographed by hikers (Fig. 5F). Three published photographs (http://tirol.orf.at/stories/522404) strongly suggest that this second rockfall detached from the same scar as the first one of 6 May. Comparative analysis of photographs of Riepen talus before and after, however, show that the second rockfall was not of sufficient magnitude to modify the outline and main characteristics of the lobate snow-avalanche/scree deposit formed on 6 May; this holds also for the number and distribution of boulders (see below). It is assumed that during the second event much or most of the rockfall material was battered to dust and sand-sized material while clashing down the summit canyon. After this second event, again, rockshowering typically weakened during the night and increased from *ca* 09:00 to 10:00 hours. Rockshowering, overall, gradually faded out over a period of months. After seven field visits, the first day witnessed as practically devoid of rock showers was 16 September 2011. On that day, the apex of Riepen talus was sampled. The last field visit in 2011 was on 5 October. At that time, despite significant volume loss by meltdown, some of the avalanche snow underneath the scree still had not completely melted; the snow had metamorphosed into a compact, frozen mass of firn that was impossible to penetrate with the avalanche sounder. In October 2011, in other areas of the Kalkkögel range, snow from the previous winter had melted completely. During the snow-rich winter of 2011/2012, snow cover accumulated that was contiguous until about the end of April 2012.

DEPOSIT

Initial features

The features documented on the day of the rockfall event until the first field trip on 11 May 2011 are subsumed as 'initial' features of the deposit. Shortly after the event, the surface of the deposit showed: (i) a relatively wide, elongate, central part of scree and scree mixed with snow (Figs 5B, C and 6A); and (ii) elevated levées of avalanche snow mixed with scree. These levées extended down from the proximal part of Riepen talus, increased in height and width downslope, and merged with a distinct frontal part of the avalanche (Fig. 5D). Wherever tested, the scree/snow-avalanche deposit showed a two-layer composition of: a lower layer A of pure avalanche snow, veneered by an upper layer B of snow mixed with rockfall-generated scree of clay-size to boulder-size sediment (Figs 6B, C and 7). Both on 6 May and during the first field trip on 11 May, however, most of the rockfall-related boulders in layer B barely protruded from the snow (Figs 6 and 7). Only a few boulders projected distinctly above the scree-laden snow (Figs 5C, D and 6A). Boulders more than *ca* 4 to 5 m in width, and that were located on the slope before the rockfall event, had remained in place while being spilled over by the avalanche (Fig. 6A). In the distal part of the deposit, soundings at numerous locations with a 4·2 m avalanche sounder did not reach ground. On the other hand, exposure of pre-rockfall boulders along the snout of the avalanche suggested that the distal part of the avalanche was up to *ca* 5 to 7 m in thickness. The observation that the sounder could be pushed down into the avalanche snow over its entire length, without reaching an obstacle, confirms that layer A was devoid of lithoclasts at least down to near its base.

In the apical to proximal slope sector of Riepen talus, the snow cover beyond the margins of the scree/snow-avalanche was veneered with a 'stray' of angular, medium pebble-sized to sand-

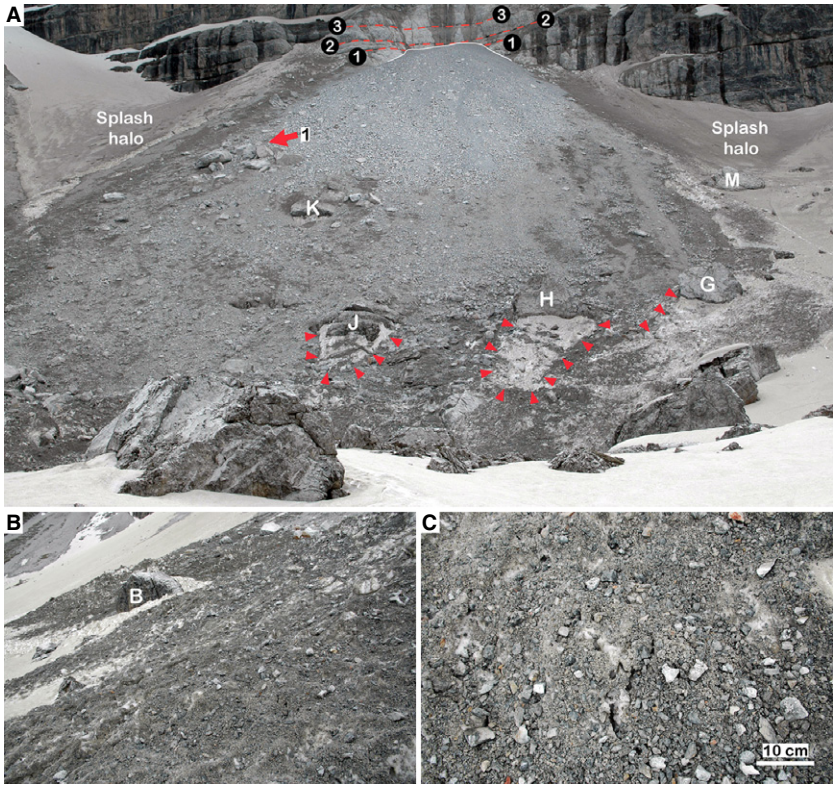

Fig. 6. (A) Overview of the avalanche deposit on 11 May 2011, five days after the event. Note: (i) cluster of boulders (red arrow labelled 1) emplaced during the event (cf. Figs 2 and 5); and (ii) avalanche 'flow shadows' (outlined by red arrowtips) downward of pre-6511 rockfall boulders 'G' to 'J', exposing avalanche snow (avalanche layer A, see text). Red-dashed bedding surfaces labelled 1 to 3 sustained an estimate of aggradation in the apical part of Riepen talus (cf. Fig. 14). (B) Northward view along the snout of the 6511-avalanche deposit, 11 May 2011. Avalanche snow veneered with melted-out scree represents the distal fringe of the event deposit. Width of view in the foreground *ca* 5 m. (C) Surface of distal part of 6511-avalanche, 11 May 2011. Unsorted scree melting out from snow of avalanche layer B.

sized lithoclasts embedded in a fine-grained matrix of rockfall-derived material (splash haloes indicated in Figs 2B, 5C and 6A). In addition, a few small 'outrunner' boulders less than *ca* 1·5 m in diameter with unweathered, freshly produced fracture surfaces were found downslope beyond the front of the 6511-avalanche. The helicopter photographs are of a high enough resolution to show that at least a few of the boulders had bounced and slid down on top of the scree/snow-avalanche deposit shortly after its emplacement (Fig. 5C and D).

Post-depositional changes, 2011

According to accessibility in the wake of the rockfall, the post-event changes of the deposit are described in upslope order from the distal to apical part of slope. In the distal part, the first change was rapid meltout of scree from the surficial avalanche layer B of scree mixed with snow (Fig. 6). This change was probably propelled by moderately intense rain from a weather front passing on 8 May, followed by exceptionally warm weather from 8 to 13 May 2011. With the progressive disappearance of its matrix of snow, and with progressive downmelting of the underlying pure snow, the clastic material of avalanche layer B merged into a continuous, clast-supported drape containing material of cobble-size to clay-size grade. The drape typically ranged from 10 to 30 cm in thickness. The snow matrix of layer B everywhere had melted completely by 26 June (second field trip), while the underlying, pure snow of avalanche layer A was still undergoing melting. A comparison of field photographs from 6 May, 11 May and 26 June suggests that layer B originally was between *ca* 50 cm to perhaps 200 cm in thickness. In the months after the event, wherever excavations in the distal part of the avalanche deposit were made, the same layering was revealed: a surficial layer B of unsorted scree of grains of clay-size to boulder-size, sharply underlain by layer A of compacted avalanche snow with slide planes subparallel to local slope dip. In addition, melt-back of avalanche snow away from the flanks of pre-6511 rockfall boulders resulted in gashes that revealed the two-layer internal structure of the scree/snow-avalanche (Fig. 7A and B). Notably, avalanche layer B *initially* did not show an inverse grading of the clay-sized to boulder-sized sediment fraction (cf. Fig. 6B and C); during snowmelt, however, layer B developed inverse grading (Fig. 7C and D). From May to August 2011, the avalanche snow metamorphosed from

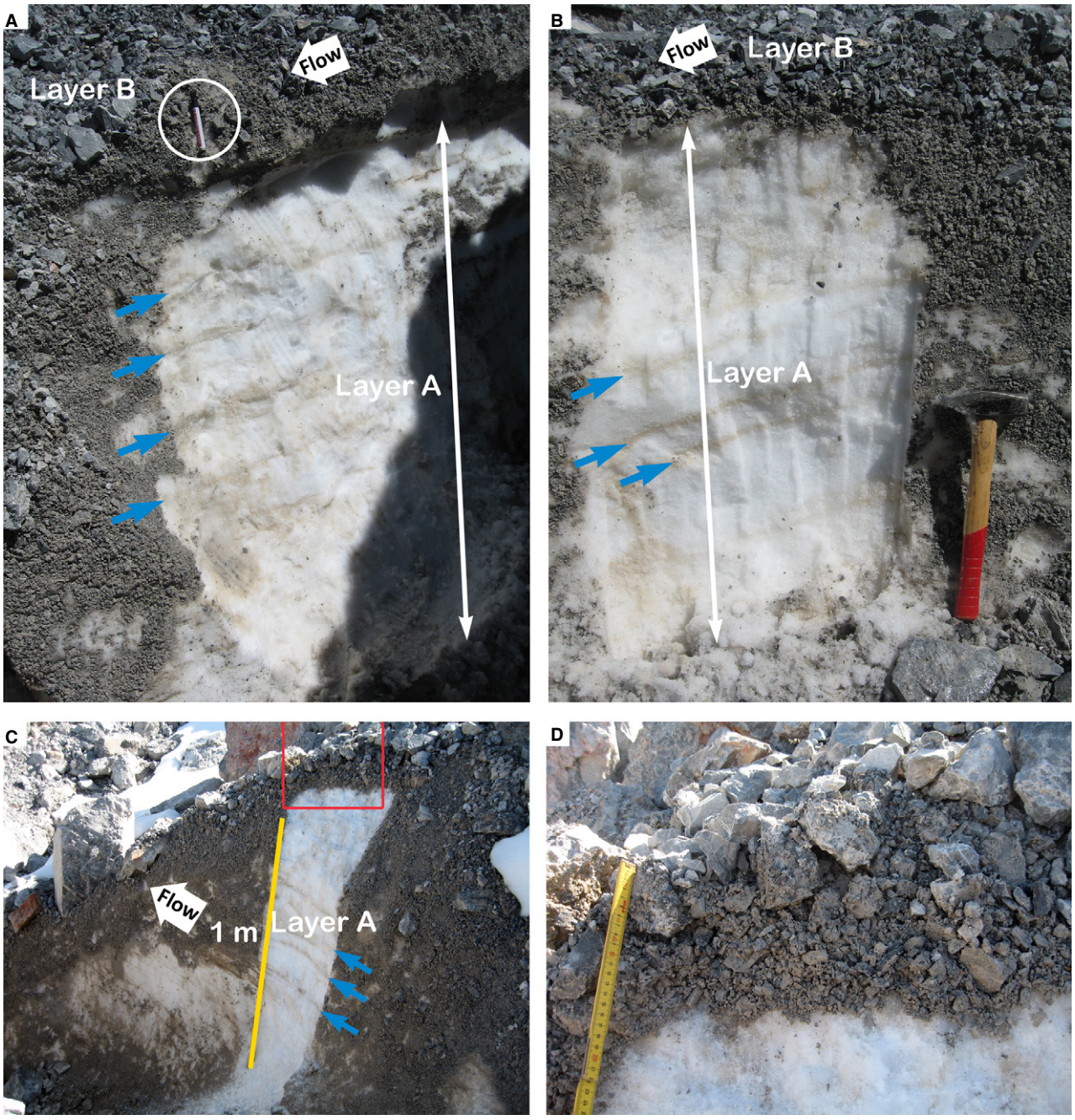

Fig. 7. (A) and (B) Excavations in the distal part of the avalanche deposit, 27 June 2011. Wherever made, excavations showed a lower layer A of pure avalanche snow with slide planes (light-grey lines labelled by blue arrows), veneered by an upper layer B of scree. Layer B results from meltout of scree from a former 'scree + snow' mixture in the shallow part of the avalanche (see Fig. 5). Pen (encircled) is 14 cm, hammer is 35 cm in length. (C) Excavation into distal part of avalanche deposit on 5 October 2011, showing vertical layering similar to panels (A) and (B). Red rectangle shows area of panel (D). (D) Scree veneer with inverse grading of grain size. Scale in centimetres.

compacted corn snow that was penetrable with an avalanche sounder into icy firn. The icy firn, in turn, could be penetrated only to a depth of a few centimetres to decimetres, and this remained so until the last field visit in October 2011. Laterally variable meltdown of avalanche layer A amplified the transient surface relief of the 'scree + snow' deposit, and revealed boulders carried within layer B of the avalanche (Fig. 8A and B). In the medial part of slope, after meltdown of layer B of the avalanche deposit, the slope surface was paved with a veneer of

cobbles to small boulders up to *ca* 1 m in size (Fig. 8C).

Avalanche splash fringe

The distalmost fringe of the 6511-snow/scree avalanche was a comparatively thin veneer of snow mixed with relatively fine-grained scree (Fig. 6B). After snowmelt, this veneer was draped over the pre 6511-talus surface. Locally, the veneer contained a sizeable amount of matrix (silt-sized to clay-sized lithoclastic material; Fig. 8D); at other locations, the veneer was poor in or devoid of matrix (Fig. 8E). Meltdown of snow beneath the *splash halo* of the 6511-rockfall (cf. Figs 2B and 6C) resulted in a drape composed of rockfall-derived, angular medium pebbles to matrix (Fig. 8F).

Avalanche margins and boulders

The elevated rims or margins of the 6511-avalanche showed internal features and a stratigraphy analogous to the distal part of the deposit (Fig. 9A). As mentioned, initially, a relatively large number of boulders up to *ca* 2·5 m in size within the distal part of the avalanche was hidden within the snow of avalanche layer B. Snowmelt revealed a loose 'scatter' of 6511-boulders that came to rest on the distal part of slope, yet none was carried to the distalmost fringe of the original avalanche (Fig. 8A and B). Locally, clusters of boulders were observed (Fig. 9B). With snowmelt, then, the 6511-boulders projected above the surrounding deposit, and were supported by the melting avalanche snow. Snowmelt resulted in transient fabrics with boulders perched in precarious positions (Fig. 9C). With the melting of avalanche layer A, boulders not only sank vertically down, but also crept downslope for at least a few metres (Fig. 9D and E). With gradual disappearance of the supporting snow, a few of the boulders further disintegrated along joints within the first months after the rockfall event (Fig. 9F).

Proximal to apical part

Relative to the distal part where early post-depositional changes are confined to effects induced by snowmelt and rain, the proximal to apical part of Riepen talus showed more significant changes subsequent to the 6511 event. Comparison of the helicopter photographs of 6 May 2011 with later field photographs suggests that, immediately after the event, the apex was of coarser-grained and more poorly sorted composition than it was later. Until about June 2011, due to a hail from numerous smaller rockfalls and ephemeral, stone-laden run-off out of the summit gorge, the apex turned into a dull-cone shape that showed a clear-cut downslope increase, or downslope grading, from small mean grain-size upslope to larger mean grain-size downslope. Until about June 2011, the apex consisted of relatively fine-grained material up to coarse pebble size. Furthermore, its external appearance suggested that it was richer in silt-sized to clay-sized matrix than the more distal parts of the slope. In addition, until about June 2011, the apex was devoid of linear erosion by surface run-off as characteristic of, both, the pre-6511 apex (see Fig. 2A) and its state a few months after the rockfall event. After June 2011, as mentioned, the frequency and volume of smaller rockfalls gradually faded out, and the apex started to become re-shaped by: (i) linear erosion from surface run-off, in particular along the contact to Riepenwand cliff; combined with (ii) deposition of tongues of openwork pebbles to cobbles; and (iii) by formation of a veneer of fresh, rockfall-derived pebbles to cobbles on a layer up to *ca* 5 cm thick, and concordant with the talus surface, of firm, cohesive sand rich in matrix of silt-sized to clay-sized material. On 16 September 2011, when the apex could firstly be accessed, it consisted of well-sorted fine pebbles to coarse sand with a matrix of cohesive carbonate mud (Fig. 10A).

Dust halo

On the first field trip (11 May 2011), the rockfall dust had coalesced into mammillary to sub-globular aggregates up to one centimetre in width. This aggregation was observed both on the snow cover and on the leaves and shoots of mosses and plants. With the passing weeks, the dust was progressively washed by rain onto the underside of rockfall pebbles to boulders, where it formed mammillary to vein-like draperies up to a few millimetres in thickness (Fig. 10B). Beyond the 6511-avalanche deposit, on boulder surfaces facing the sky, the dust was washed into small puddles by rain. In addition, after snowmelt, the dust was coalesced to mammillary aggregates on clast surfaces (Fig. 10C), and was moulded to small patches on vegetated soil (Fig. 10D). A second significant production of rockfall-related dust took place on 21 June; this input, however, occurred when the talus was devoid of snow exposed at the surface (Fig. 5F). Input of dust produced by frequent smaller rockfalls, however, continued at least until approximately July 2011.

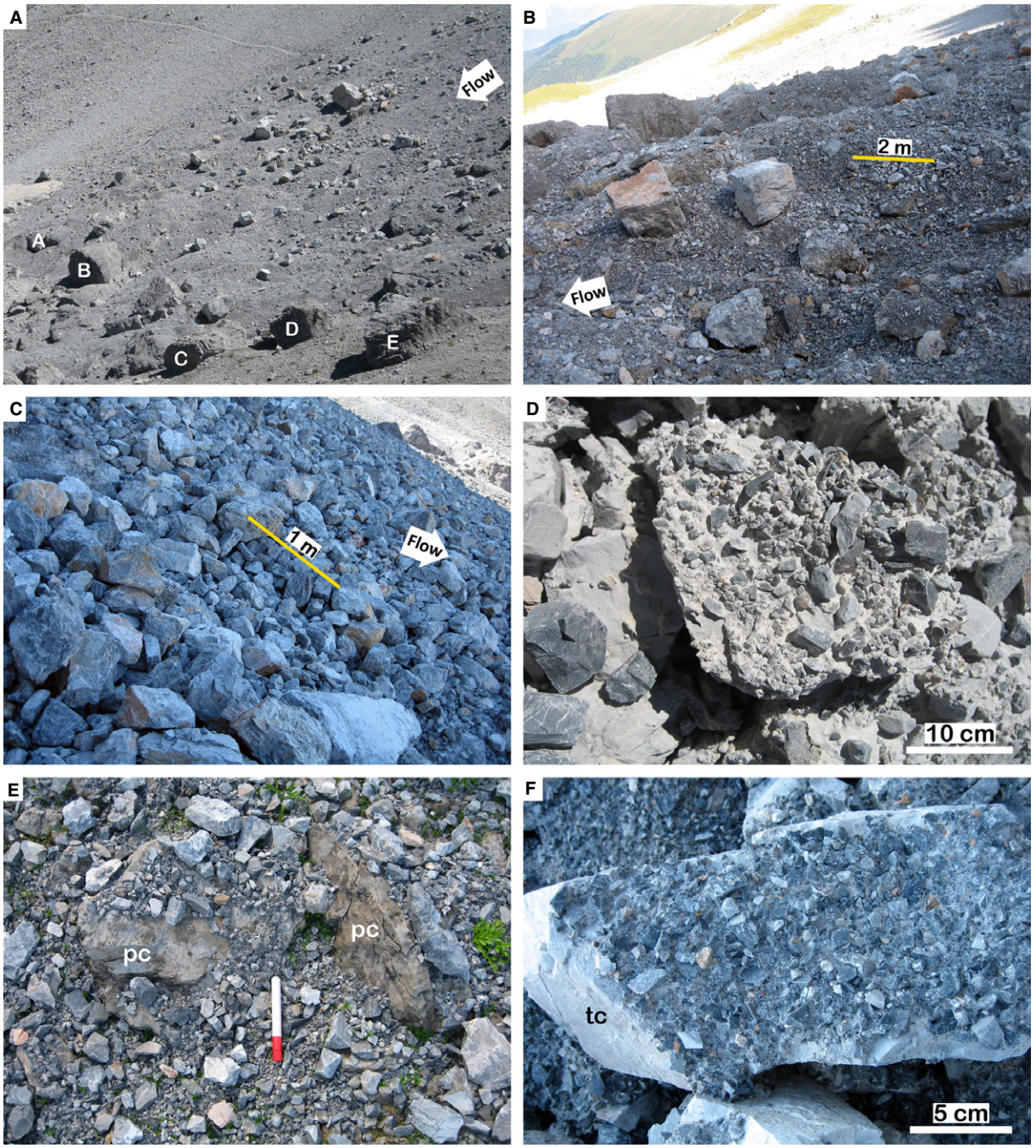

Fig. 8. (A) Northward view over the distal part of the avalanche deposit, 18 August 2011. The rugged topography results from underlying avalanche snow, not sediment. Width of view in middleground *ca* 60 m. (B) Northward view over the distal part of the avalanche deposit. Rugged surface is from underlying, downmelting, pure avalanche snow (layer A); 18 August 2011. (C) Southward view over proximal segment of Riepen talus, consisting of a veneer up to a few clasts in thickness of cobbles to small boulders derived from the 6511-rockfall and its aftermath; 16 September 2011. (D) Distal fringe of the avalanche after local snowmelt, 27 June 2011. Very-poorly sorted rockfall clasts and intercalated, light-grey veneer of fine-grained matrix of clastic carbonate mud (silt-sized to clay-sized sediment). (E) Lateral fringe of avalanche after snowmelt, 18 August 2011. Note: (i) shrubby vegetation of pre-6511 talus surface; and (ii) difference between brownish-weathered, lichenized pre-6511 rockfall clasts (pc) with litter of light-grey, angular, unlichenized clasts transported to the site by the avalanche. Pen: 14 cm. (F) Detail of left-side splash halo after snowmelt, 6 July 2011. Pre-6511 talus cobble (tc) veneered by rockfall-derived sediment of clay to medium pebble size. The pebbly sediment fraction throughout consists of angular unlichenized rock fragments, embedded on a cohesive matrix of clastic carbonate mud.

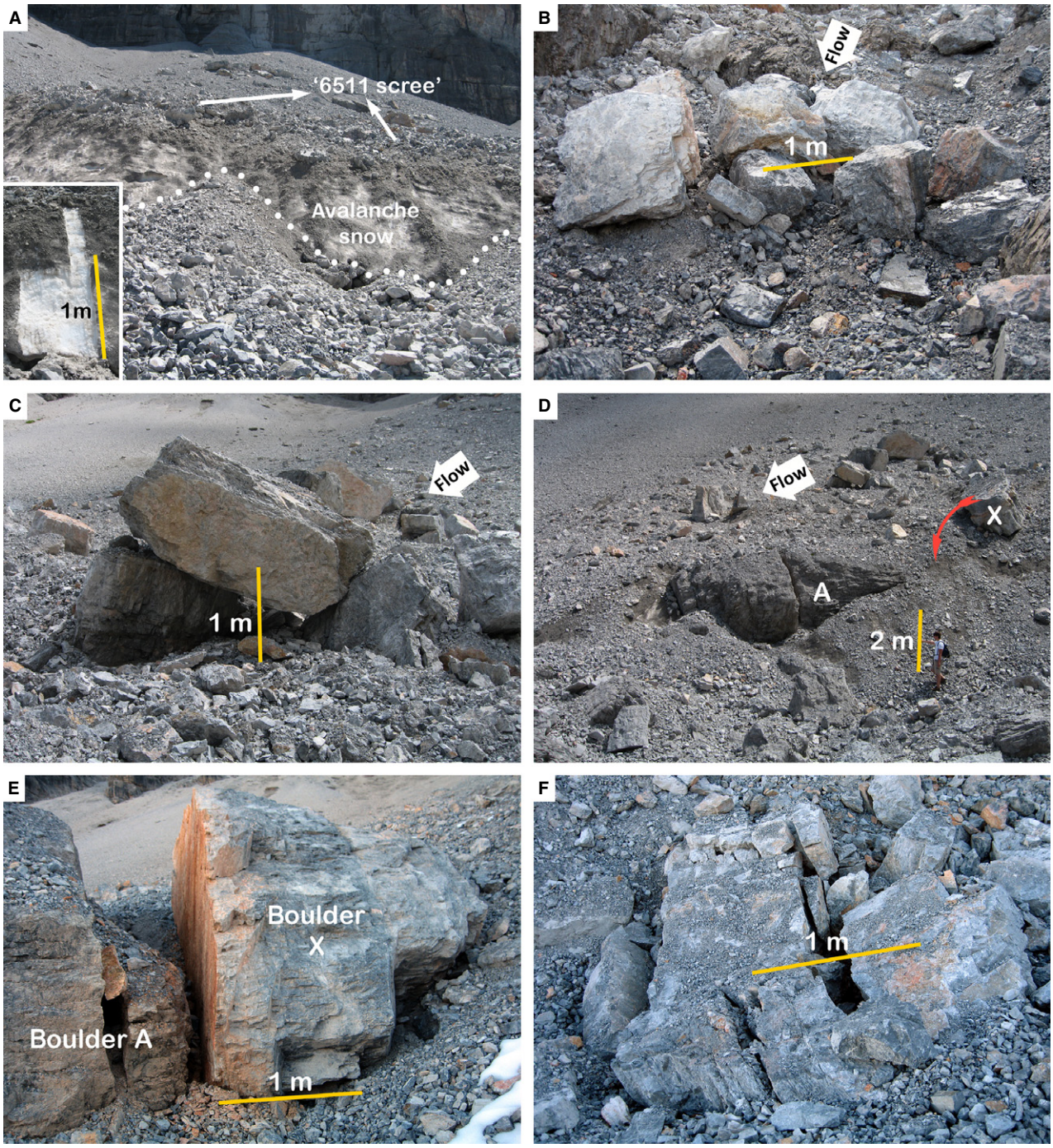

Fig. 9. (A) Upslope view of the backmelting right margin of the avalanche, 6 July 2011. In snowmelt, the scree veneer on top is redeposited in small cones (white stipples). Note also the layered appearance of the avalanche snow. Width of view *ca* 6 m. Inset shows excavation at site, with pure avalanche snow veneered by scree. (B) Cluster of boulders melted out of avalanche layer B, 18 August 2011. At the day of observation, these boulders and the other, laterally adjacent scree still rested on pure avalanche snow. (C) Boulder perched on two other boulders, 6 July 2011. The boulder cluster was underlain by pure avalanche snow. During later field trips, this fabric was no longer present. (D) Backmelting snout of avalanche, showing pre-6511 rockfall boulder A, 6 July 2011. Boulder X arrived with the avalanche; this boulder crept downslope for a few metres upon melting of underlying avalanche snow [see (E)]. (E) Snowmelt in avalanche layer A has led to downslope creep of boulder X, and to juxtaposition along the pre-6511 rockfall boulder A; 5 October 2011. (F) 6511-rockfall-derived boulder, disintegrated *in situ* upon downsinking with snowmelt, 5 October 2011. Note the fitted boundaries of open fractures.

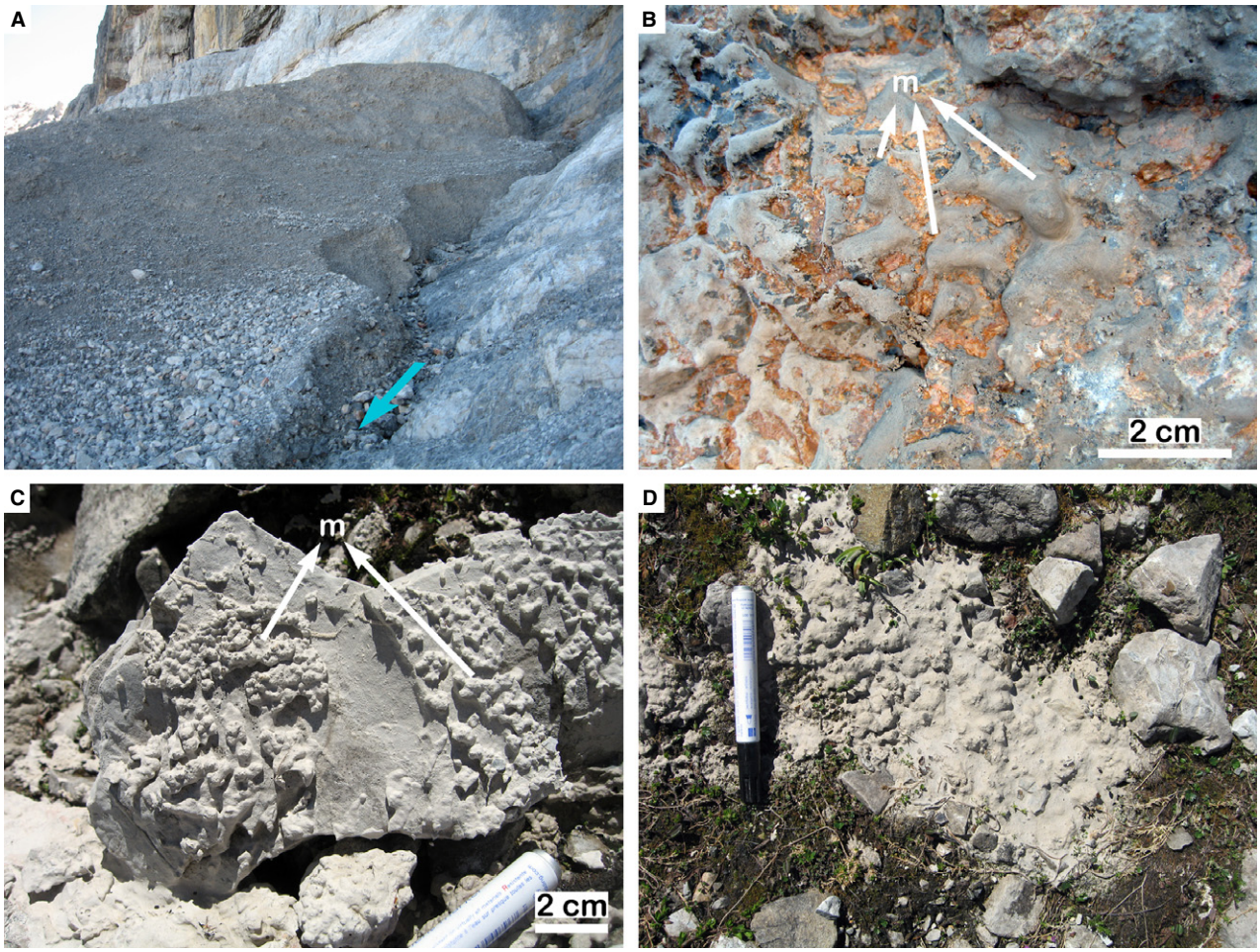

Fig. 10. (A) Apex of Riepen talus, 16 September 2011. Note the composition of the relatively well-sorted, fine-grained, cohesive material. The small trench (blue arrow) resulted from beginning re-incision by ephemeral surface run-off from the south-west summit gorge of Riepenwand (cf. Fig. 3). Width of view in middleground *ca* 6 m. (B) Underside of rockfall boulder of 6511-avalanche deposit, with aggregates of fine-grained rockfall material ('matrix', labelled m) illuviated by snowmelt and rain; 18 August 2011. (C) Pre-6511 talus clast, beyond the snow avalanche, littered with aggregates of rockfall-generated dust ('matrix', labelled m). The dust had aggregated upon snowmelt; 27 June 2011. (D) Detail of vegetated surface beyond the 6511-snow avalanche, 27 June 2011. After snowmelt, rockfall dust initially fallen out onto snow cover is redeposited by ephemeral overland flow into patches. Pen is 14 cm long.

Scanning electron microscope investigation

In the distal part of Riepen talus, in SEM, two samples (collected on 27 June 2011) of the rockfall-produced matrix of avalanche layer B show an extremely poorly sorted mixture of grains of mini-micrite (carbonate particles <1 μm; Folk, 1974) to sand (Fig. 11A). In the sediment fraction smaller than *ca* 20 to 30 μm, nearly all grains are of very angular shapes, and many show sharp edges and acute apices resulting from fracture (Fig. 11B). A small proportion of the particles, however, are partly or largely bounded by surfaces of the dolomite rhombohedron (Fig. 11C). No or only inconclusive indications of modification of particle shape by dissolution or precipitation were observed (Fig. 11B to D). *In situ* energy-dispersive X-ray fluorescence analyses suggest that the mini-micritic particles also consist of dolomite. In all inspected samples of 6511-rockfall matrix, indications of chemical dissolution such as honeycomb structure, pitting and dissolution channels were very rare.

Two samples collected on 27 June 2011 of rockfall-generated *dust* from: (i) a small puddle on top of a boulder located south-west off Riepen talus; and (ii) from a snow patch *ca* 10 m ahead of the front of the 6511-rockfall deposit, showed

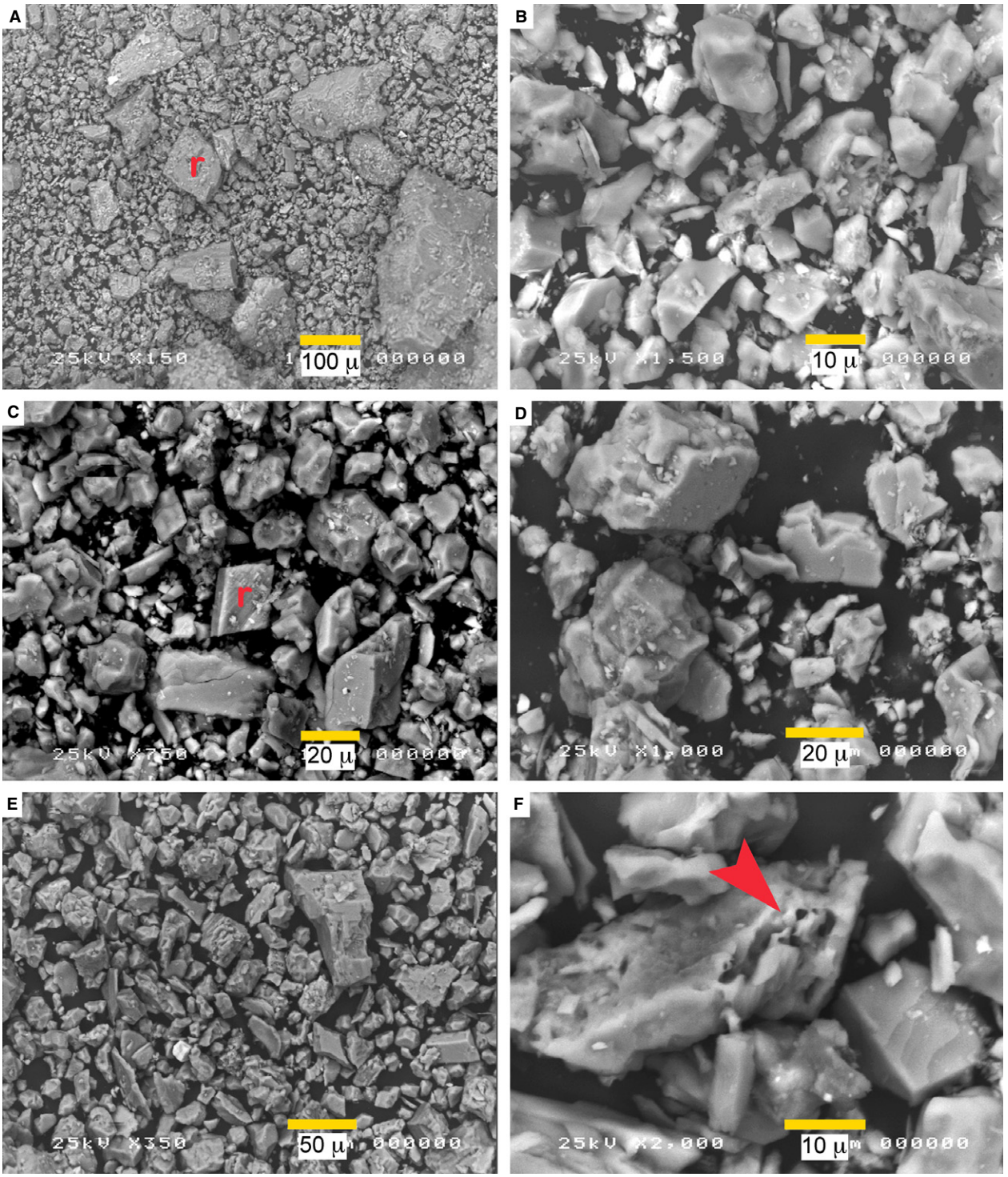

Fig. 11. (A) Sample of fine-grained matrix of apex of Riepen talus, taken on 16 September 2011. Note: (i) extremely poorly sorted composition; and (ii) grain of sub-rhombohedral shape (labelled r). (B) Detail of sample in panel (A): Extremely poorly sorted sediment composed of angular fragments of silt-size to clay-size grade. (C) Sample of apex of Riepen talus, 16 September 2011. Note the extremely poorly sorted composition, and grain of rhombohedral shape (labelled r). (D) Detail of sample in panel (C): Particles are bounded by surfaces according to the dolomite rhombohedron (crystal surfaces and cleavage surfaces), and by fracture surfaces of irregular shape. (E) Sample of rockfall dust fallen out on top of an older boulder beyond the snow avalanche. Apart from being composed of very angular particles, this sample appears relatively better-sorted than those of panels (A) to (D). (F) Detail of sample in panel (E): Grain with pitted surface (red arrowtip).

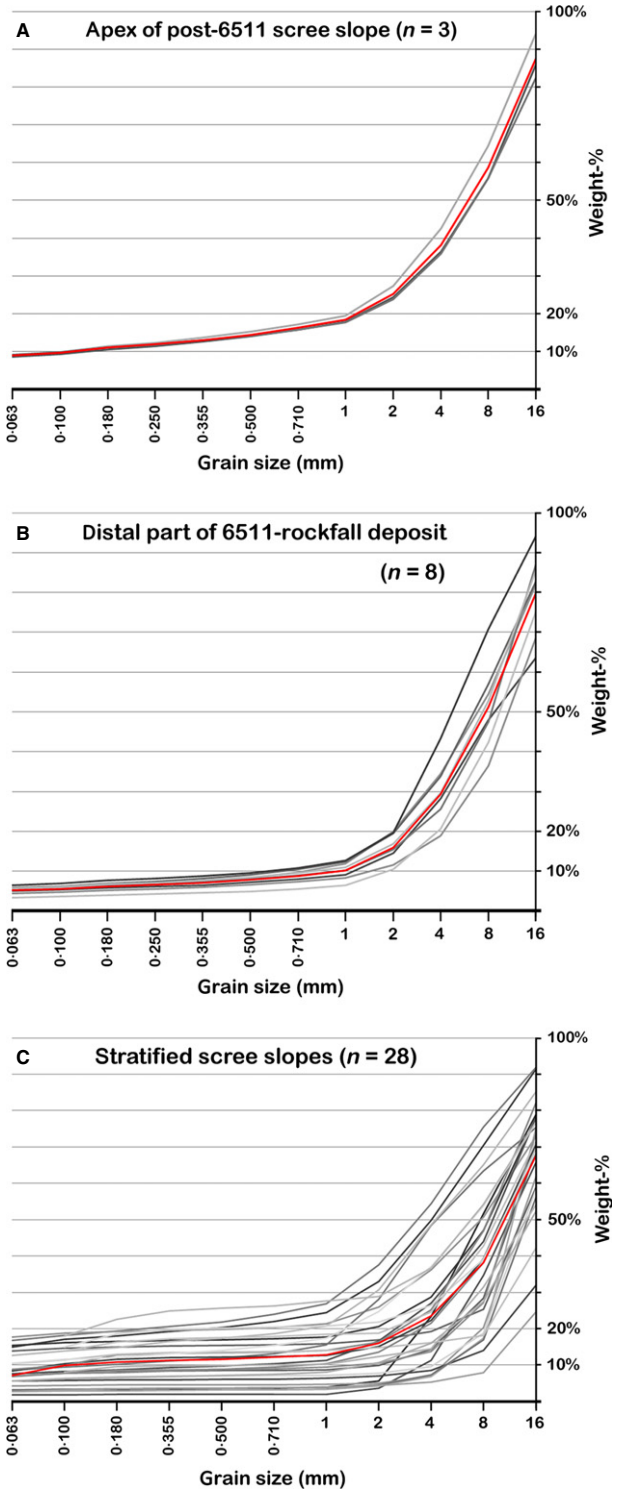

Fig. 12. Grain-size distributions (weight per cent) of sediment fraction ≤16 mm of: (A) apex of post 6511-scree slope (samples from 16 September 2011); (B) of distal part of 6511-avalanche (samples from 11 May 2011 and 27 June 2011); and (C) of excavations into stratified scree slopes of the Kalkkögel range. The average is indicated by a red line. See text for discussion.

characteristics that differed from those of the matrix. In both dust samples: (i) micritic to mini-micritic particles seemed to be more rare than in the matrix samples; (ii) the mineralogical composition is more diverse and includes calcian dolomite, potential dedolomite or magnesian calcite, calcite and blade-shaped particles composed mainly of Si, Al and O (probably phyllosilicates); and (iii) many carbonate grains (dolomite, dedolomite/Mg-calcite and calcite) show pitting and channelling (Fig. 11E and F).

Grain-size distribution from wet sieving (fraction ≤16 mm)

The composition of the sediment fraction ≤16 mm of the apex of Riepen talus and of the distal part of avalanche layer B were compared to samples from stratified talus slopes of the Kalkkögel range (Fig. 12). Note that the scree sampled from the apex on 16 September 2011 (Fig. 12A) is *younger* than the sediment sampled from avalanche layer B (Fig. 12B). This is because the apex had re-built during the many smaller aftermath rockfalls; in addition, surface run-off from the summit gorge during rainstorms contributed significantly to buildup of the apex in the months between the main rockfall event and the day of sampling. As mentioned, in avalanche layer B, an overwhelming number of sand-sized to boulder-sized lithoclasts were fresh, rockfall-derived material. It thus can be safely assumed that the sediment of layer B stems, entirely or nearly, from fracturation during the rockfall rather than representing sediment reworked from the overridden part of Riepen talus. In layer B, a significant yet unquantified portion of the carbonate mud (silt-size to clay-size grains) probably stems from settled dust of the numerous smaller scale rockfalls in the weeks after the main event, with the 'dust-rich' rockfall of 21 June perhaps the most prominent one. Despite the differences in origin and relative time of sampling, the sediment fractions ≤16 mm from both the apex and the distal part of layer B are similar with respect to: (i) the relative grain-size distributions, with low sand content (flat part of curves) and a significant increase in percentage of pebbles (≤16 mm, sharply steepening part of curves); and (ii) a content of mud ≤0·063 mm in grain size between 4 wt% and 9 wt%. In the sediment fraction ≤16 mm, samples from excavation into stratified scree slopes of the western face of Kalkkögel range show much wider variability (Fig. 12C). The large variability in the scree-slope samples

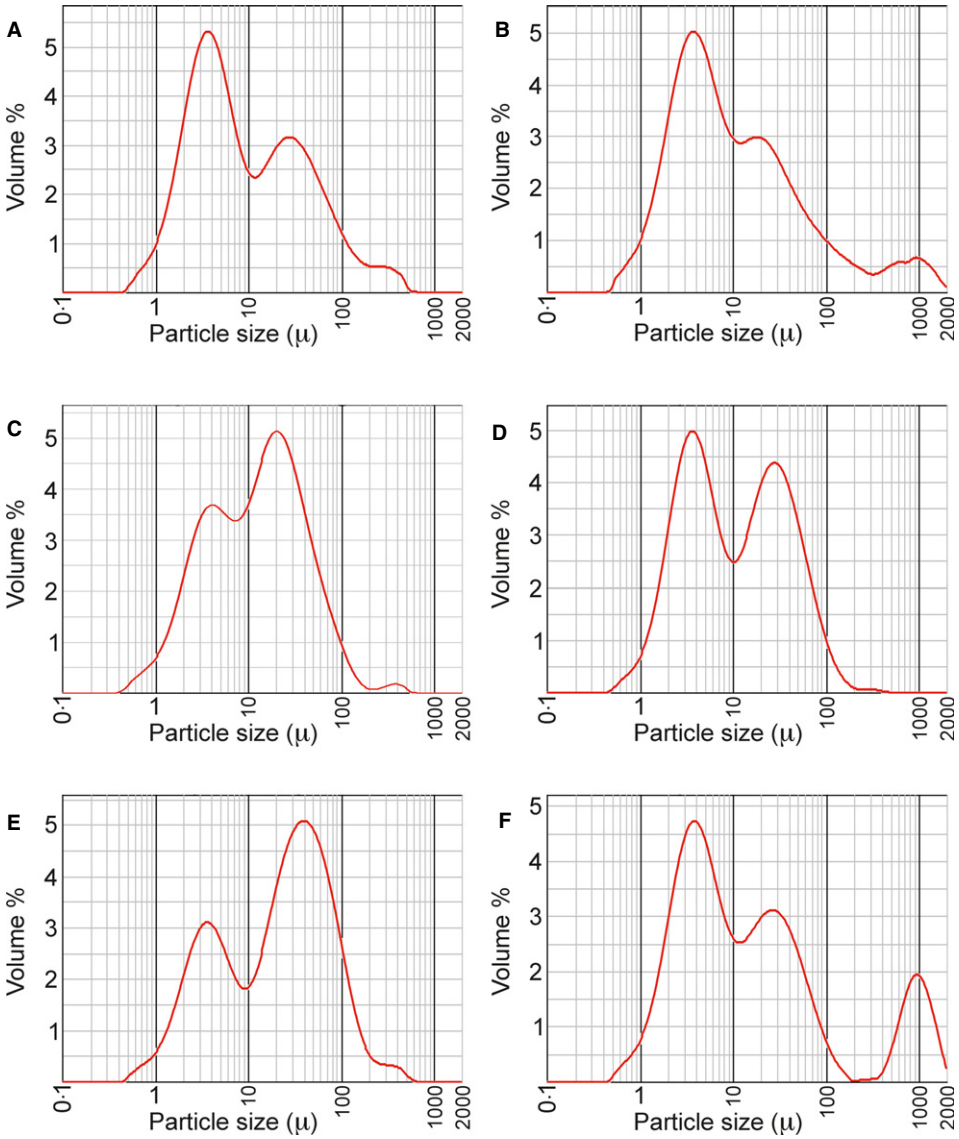

Fig. 13. Malvern® mastersizer grain-size distributions of sediment fraction ≤2 mm of: (A) distal part of layer B of 6511-snow avalanche; (B) apex of Riepen talus; (C) 6511-rockfall-generated dust fallen out on snow beyond the avalanche; and (D) to (F) excavations into stratified talus slopes of the Kalkkögel range. See text for discussion.

results from the fact that stratified slopes are subject to a host of processes (for example, debris flows, particle creep, frost heave, ice segregation, growth of needle ice, stripping of surficial pebble veneer by snow avalanches and snow glides, illuviation/eluviation of matrix during snowmelt and rain, etc.). Nevertheless, the individual grain-size distribution curves and, in particular, the average of all curves are remarkably similar to those of the apex and of layer B. The average content of 7 wt % of matrix in the stratified talus slopes is in a similar range to that of the pristine rockfall-derived materials.

Grain-size distribution from laser diffraction analysis (fraction ≤2 mm)

From the distal part of the 6511-deposit, two samples were subject to laser diffraction analysis (Fig. 13A). The results show: (i) absence of particles <0·4 μm; (ii) a peak in relative percentage of grains between *ca* 2 to 8 μm in size; and (iii) a second smaller peak of grains a few tens of microns in diameter. The measurements thus suggest a bimodal grain-size distribution with a lower cut-off at 0·4 μm. From the apex of Riepen talus, two samples of matrix (col-

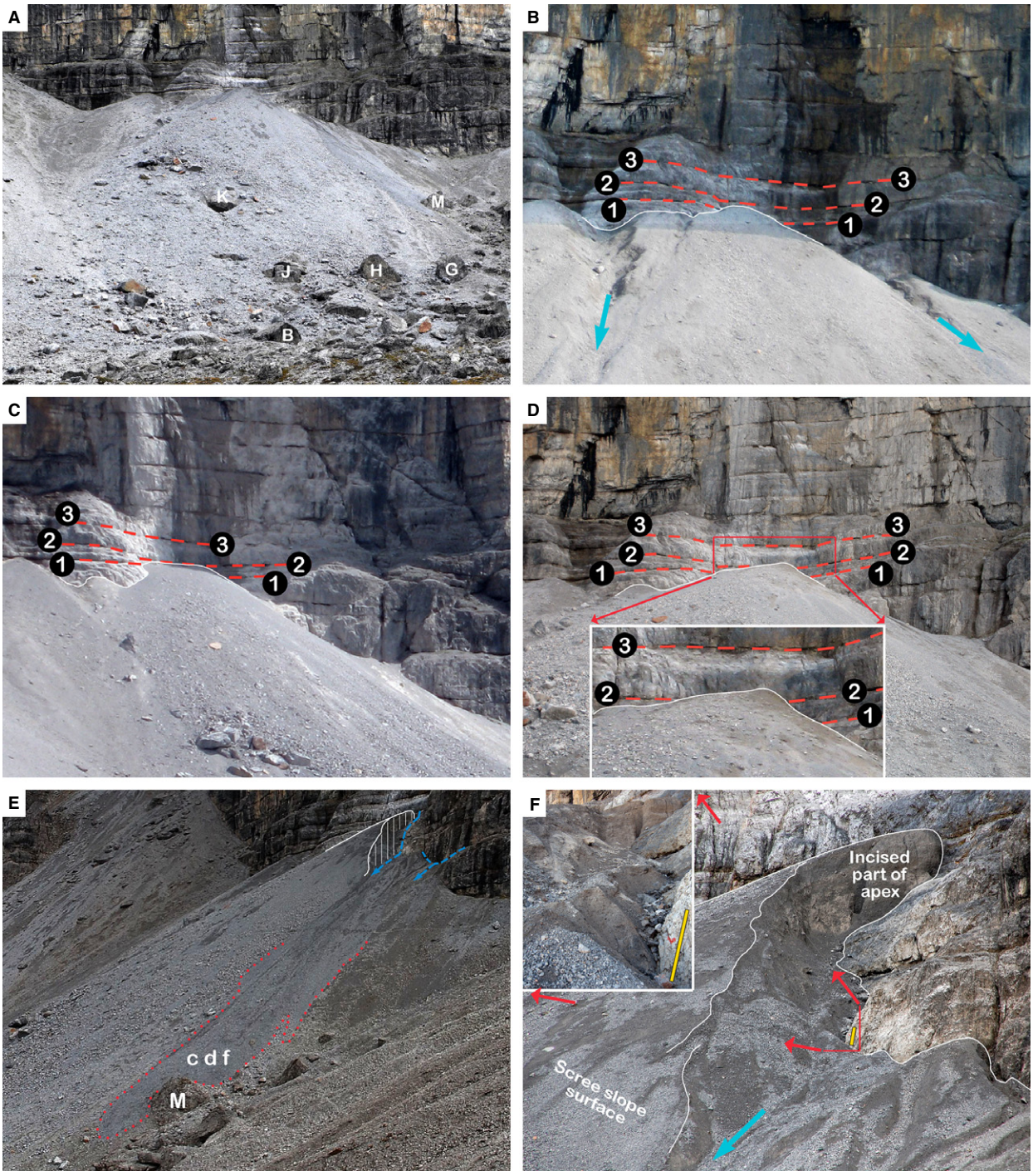

Fig. 14. (A) Overview of Riepen talus, 18 September 2012, with pre-6511 rockfall boulders labelled by letters (cf. Fig. 2). (B) Talus apex on 12 September 2010, i.e. eight months before the rockfall event (cf. Figs 2 and 3). The red-dashed bedding surfaces 1 to 3 indicate that the 6511-rockfall had led to only minimal aggradation of the apex [compare panel (C)]. Note also the incised chutes (labelled by blue arrows) produced by ephemeral surface runoff from the summit gorges of Riepenwand. (C) and (D) Status of talus apex on 29 June 2011 (C) and 18 August 2011 (D). The incised chutes that flanked the apex prior to the 6511-rockfall were filled up. Bedding planes 1 to 3 indicate that the vertical aggradation of the apex was a few metres only. (E) Northward view onto Riepen talus, 5 October 2012, with pre-6511 rockfall boulder 'M'. The apex was subject to re-incision (white vertical lines). The eroded scree was redeposited in lobes composed of cohesive debris-flow deposits (cdf, outlined by red dots). (F) Detail of the apex undergoing re-incision, 3 October 2012. Inset (enlargement indicated by red arrows) shows view up the re-incised chute, with a red trailmark on the rock. Scale bars are 1 m.

lected on 16 September 2011) were analysed (Fig. 13B). Overall these samples show a grain-size distribution, relative percentage of grain-size classes, and lower grain-size cut-off quite similar to that of the samples from the distal part. From the dust fallout, two samples were analysed: these also show no particles smaller than *ca* 0·4 μm, but differ from the matrix samples by a main peak in grains a few tens of microns in size (Fig. 13C). To sum up, the two common features of the grain-size distributions of rockfall-generated matrix and the dust fallout are: (i) a lower size limit at 0·3 to 0·5 μm; and (ii) a bimodal size distribution with one peak at a few microns grain size and another peak at a few tens of microns. For comparison, five samples of matrix from excavations into stratified talus slopes of the western face of the Kalkkögel massif were analysed. These samples show: (i) absence of particles smaller than *ca* 0·4 μm; (ii) a bimodal grain-size distribution with peaks located in the same size ranges (few microns, few tens of microns) as in the samples of rockfall matrix and dust; but (iii) a variable grain-size range of peak volumes (Fig. 13D to F). Despite the wider range of matrix contents of stratified talus, however, the persistence of both the lower grain-size cut-off at *ca* 0·4 μm and the presence of two peaks in the grain-size range from a few microns and a few tens of microns are noted.

Year after (2012)

As mentioned, along the distal fringe of the 6511-avalanche, the snow had not melted completely before the onset of the successive cold season 2011/2012. The status after complete snowmelt (documented on 18 September 2012) is summarized as follows. Overall, the outline of the 6511-deposit still was clearly identifiable (Fig. 14A). In the distal part of the deposit that was underlain by snow on 5 October 2011, the scree veneer on top of the avalanche was laid down onto the pre-6511 talus surface. Over most areas, this resulted in a veneer of angular, unweathered scree of sand-sized to very coarse pebble size sediment littered with cobbles to small boulders. In patches, the veneer is just a 'loose stray' of 6511-clasts on the older talus surface; this is recorded by weathered, lichenized clasts and shrubby vegetation peeking through the 6511-scree litter. Where the original avalanche snow had positive relief, snowmelt led to a veneer of unsorted pebbly to cobbly scree up to 30 cm in thickness. Otherwise, no changes were evident in the distal part of the slope.

A more marked change since 2011, however, had taken place in the apical to proximal part of the slope. Before the rockfall, the apex was delimited on each side by an erosionally incised chute (Fig. 14B). After the rockfall, these chutes were filled up with scree, whereas the uppermost tip of the apex aggraded only slightly (Fig. 14C and D). Subsequent to approximately early August 2011, the apex became erosionally re-incised by surface run-off out of the same summit gorge that had spouted the 6511-rockfall. Apical re-incision corresponds with growth, mainly over spring and summer 2012, of a lobe of cohesive debris-flow deposits on the proximal part of slope (Fig. 14E). Field inspection of the incised apex allowed estimation of vertical aggradation along the incised chute due to the 6511-rockfall. Incision had re-exposed a red landmark of a climbers' trail along the toe of Riepenwand (Fig. 14F, and inset). Because this landmark is painted onto the rock *ca* 1 to 1·8 m above the pre-6511 talus surface, it provides a proxy indicator of the former surface of the incised chute. Comparative analysis of scaled field photographs thus indicates that the incised chute in the apical part of slope had aggraded vertically by *ca* 5 to 6 m during the 6511-event and its aftermath. Conversely, the left-side splash halo showed no marked changes until 18 September 2012.

INTERPRETATION AND DISCUSSION

Rockfall trigger

As mentioned in the *Seismic activity* section, there is no evidence that the 6511-event was triggered by seismic activity. The rockfall, however, was preceded by three successive months with an average temperature distinctly above the 1971 to 2000 mean (Fig. 4A). Although the detached 'flake'-shaped rock mass was a few metres in thickness only, thermal conductivity of rock is not high enough for three months of relative warming to arrive at a depth of a few metres within the rock mass (cf. Gruber *et al.*, 2004; French, 2007). Permafrost warming to temperatures closely below the freezing point, however, terminates the 'cementing effect' of ice (Davies *et al.*, 2001; Nötzli & Gruber, 2005; Gruber & Haeberli, 2007; Ravanel *et al.*, 2010). If perma-

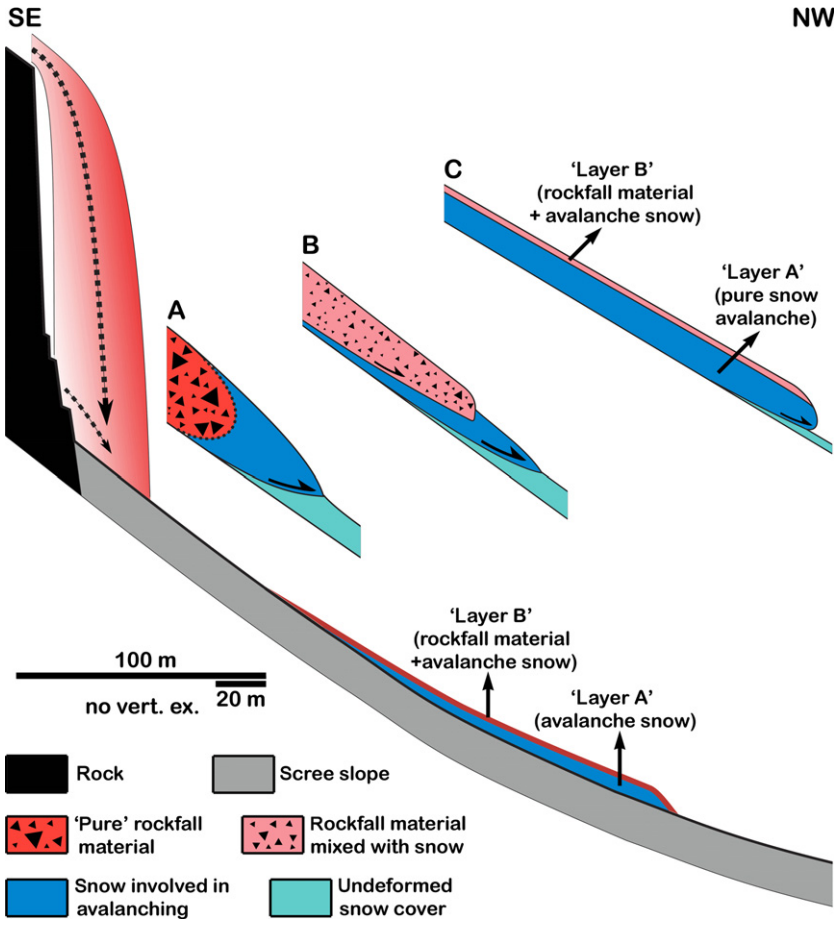

Fig. 15. Development of a rockfall-triggered two-layer avalanche. (A) Impact of the rock mass churned up the snow cover down to ground, and a mass of rock fragments mixed with snow started to push laterally outward and downslope. In an early stage of downslope movement, the snow cover closely ahead of the moving mass of 'scree + snow' was sheared off and entrained. (B) Further entrainment of snow by detachment in the headward region of the avalanche increased the mass of snow relative to rockfall material. (C) When fully developed, the avalanche consisted of a comparatively thick layer of snow (layer A) overridden by a layer of 'scree + snow' (layer B).

frost weakening (not necessarily melting) indeed played a role, the required warming may reflect a longer term signal beyond three months in duration. The anomalously warm spring in 2011 may have aided in rockfall detachment: in cliffs, meltwater percolating down vertical fractures accelerates strongly permafrost decay, favouring rockfall (Matsuoka & Sakai, 1999; Krähenbühl, 2004; Gruber & Haeberli, 2007). Temperature gauges are not available for the summit gorges of Riepenwand, but the gorges are located near the *gross* lower limit (2500 to 3000 m a.s.l.) of continuous permafrost in the Eastern Alps (Kneisel, 2010). In shady locations or under otherwise favourable circumstances, permafrost can be present down to 2500 m a.s.l. or even lower (Nötzli & Gruber, 2005; Lambiel & Pieracci, 2008; Kneisel, 2010). Permafrost weakening and/or percolation of meltwater along vertical fractures thus potentially triggered the 6511-rockfall. It is however remarked that even in areas with long detailed rockfall monitoring, such as the Yosemite National Park (USA), only half of all events can be referred to a trigger such as intense rainfall or an earthquake (Zimmer *et al.*, 2012).

Rockfall and avalanche development

Phase 1

The rock mass involved in the 6511-event could not fall down freely, but first crashed into the summit gorge (Fig. 3). As a result of numerous impacts, the falling rock mass became intensely fragmented. The disintegrated rock mass then spouted out from the exit of the gorge, and fell down freely over some 150 m onto the apical part of Riepen talus (Figs 3 and 15). Further fragmentation, in particular of cobbles to boulders, probably took place upon this second impact.

Phase 2

Hitting the snow-covered scree slope, the mass of rockfall material pushed vigorously outwards and downslope from the impact area. As a result, the initial stage of avalanche development probably was a thorough mixture of scree and wet granular snow. The front of the forcefully driven snow-scree mixture ploughed into the pure snow cover laterally and downslope of the impact area (Fig. 15A). Due to the shear exerted by energetic flow of the snow-scree mix, the overridden pure-

snow cover detached along or near its base, and became part of the avalanche while carrying the mixed snow-scree layer piggyback (Fig. 15B). This phenomenon of snow entrainment along the avalanche front is well-known for avalanches of granular snow (e.g. Sovilla *et al.*, 2001, 2006; Sovilla & Bartelt, 2002; Kern *et al.*, 2009). In this way, an avalanche composed of a lower layer of pure, entrained snow overlain by an upper layer of scree mixed with snow formed. Snow entrainment probably took place by ploughing at the avalanche front ('frontal entrainment'), as well as some distance behind the downslope avalanche-tip ('step entrainment' or 'basal erosion') (see, e.g. Sailer *et al.*, 2002; Sovilla & Bartelt, 2002; Sovilla *et al.*, 2006; Issler *et al.*, 2008; Christen *et al.*, 2010). Wet-snow avalanches are characterized by an upper, moderately deformed layer riding on a thinner lower layer wherein most deformation is accommodated (e.g. Tiefenbacher & Kern, 2004; Sovilla *et al.*, 2008). This characterization is not 'plug-flow' *sensu strictu* (e.g. Voellmy, 1955; Savage, 1979), and hence is termed 'plug-like' flow hereafter (cf. Brugnot & Pochat, 1981; Dent & Lang, 1982; Sovilla & Bartelt, 2002; Kern *et al.*, 2004, 2009; Tiefenbacher & Kern, 2004; Thibert *et al.*, 2008; Buser & Bartelt, 2011).

Phase 3

Snow entrainment along the frontal part of the avalanche led to development of the two-fold layering as described, i.e. a lower layer of pure avalanche snow carrying piggyback an upper layer of snow plus scree. During development of this type of avalanche, basal shear exerted by downslope movement is transferred more-or-less completely from the initial scree-snow mixture (Fig. 15A) to the underlying, entrained avalanche snow (Fig. 15C). A laminar style of movement (see Pudasaini & Hutter, 2007, for terminology), at least shortly before and during halting of the avalanche, is suggested by the subparallel sliding surfaces in the lower (pure snow) part of the avalanche deposit. If moving like a laminar-type avalanche, the mass probably travelled at velocities of 5 to 25 m sec^{-1} (18 to 90 km h^{-1}; cf. Pudasaini & Hutter, 2007; Sovilla *et al.*, 2008; Kern *et al.*, 2009). Radar measurements recently showed that ground avalanches representing an apparently 'single' event may indeed descend as a series of avalanche fronts, or surges (Vriend *et al.*, 2013). If the 6511-event descended as a series of fronts, the surging flow behaviour should leave a record, such as transversal ridges and/or duplexing of avalanche layer A and layer B. Although the backmelting cleft along boulder flanks provided insight into the avalanche deposit, at no location was duplexing observed. Also on the pristine avalanche deposit, no transversal ridges or other features suggestive of surging were seen (cf. Fig. 5). The absence of morphological and sedimentological evidence for surging, however, does not necessarily indicate that it did not take place, provided that the internal stratigraphy of the final deposit with respect to layers A and B remained intact.

Shape of avalanche deposit. The teardrop-like shape of the 6511-avalanche deposit fits with experiments whereby grain collectives are released suddenly onto an open slope (e.g. De Toni & Scotton, 2005; Pudasini & Hutter, 2007). Because the main volume of the 6511-rockfall probably hit Riepen talus within a few seconds, the effect was similar to sudden material release on the slope. Rajchenbach (2002) showed that externally triggered avalanches acquire a triangular final shape. In experiments on avalanching, however, on slopes steeper than 34°, only triangular avalanches formed, irrespective of whether the avalanche was externally triggered or self-triggered (Daerr & Douady, 1999). Recall that the long upper slope segment of Riepen talus ranges from 34° to 36° in dip. The impact of the 6511-rockfall was not a minute, nearly point-sized disturbance to just trigger instability (see Daerr & Douady, 1999), but was of sizeable radius and high kinetic energy. It is thus speculated that the impact of the falling rock mass onto the snow-covered slope increased the 'opening angle' of the final avalanche deposit. The presence of boulders mainly in the distal part and along the flanks of the 6511-deposit fits with plug-flow like behaviour. Initially, homogeneous mixtures of particles of different size laterally segregate during downslope avalanching, with coarse particles migrating towards the front and flanks of plug-like flows (Iverson & Vallance, 2001; Pudasaini & Hutter, 2007). On scree slopes, boulders located mainly along the front and flanks of snow-avalanche deposits are common (Rapp, 1959; Jomelli & Bertran, 2001). From the above, the 6511-boulder cluster placed at 2360 m a.s.l. is an exception (cluster labelled 1 in Fig. 5B and C). Because the helicopter photographs show that these boulders also were emplaced that same day, it is assumed that they fell in the aftermath of the main event onto the apical part of slope, and from there perhaps slid down some distance.

Splash haloes

The described splash haloes may be explained by two processes, which are not mutually exclusive:

1 Rockfall impact onto talus produced an airblast carrying sand to medium pebbles (cf. Morrissey *et al.*, 1999). Wieczorek *et al.* (2000) described two immediately successive rockfalls (*ca* 23 000 to 38 000 m^3 in combined volume) in Yosemite Valley that fell freely over 400 m and then impacted a talus slope. Near the impact site, an airblast comparable to a hurricane blew out, as indicated by the toppled forest ahead. A sandy deposit of rockfall material comminuted upon impact extended over about 350 m downslope from the impact site. Near the impact site, up to 10 wt% of pebbles (up to 32 mm in size) was present in some sediment samples. Wieczorek *et al.* (2000), however, assumed that at least some of the pebbles may have been deposited: "from impact rather than entrainment in the cloud". A similar airblast that downed forest over hundreds of metres was mentioned by Zimmer *et al.* (2012) for the 46 700 m^3 2009 Ahwiyah Point rockfall in Yosemite National Park. Airblasts also form from rockfalls of much smaller volume. At Mount Hellhore, Switzerland, a rockfall 400 to 500 m^3 in volume, and of 100 m free fall, produced an airblast felt by eyewitnesses down in the valley (Graf & Tobler, 2008). This event indicates that the Riepenwand rockfall (5800 m^3 volume, 150 m free fall) was large and energetic enough to produce an airblast.

2 Another process that can carry out pebbles beyond impact sites is ballistic throw. During the Hellhore rockfall, pebbles were thrown out for up to 500 m horizontally from the site of rockfall breakout; a low impact angle of some of these clasts, however, suggested that their throw may have resulted from deflection and/or impact fracture of larger clasts during downward movement (cf. Graf & Tobler, 2008). Because of its impact onto the inclined talus surface, during the Riepenwand rockfall, ballistic throw of clasts may have resulted from: (i) elastic reflection of rockfall clasts on clasts of the talus surface; and/or from (ii) elastic energy released upon fracture of clasts when hitting the talus.

Scree transport

It seems notable that a plug-like flow of coarse-granular snow (density of 300 to 550 kg m^{-3}, 0 °C; Brun & Rey, 1987) has the competence to carry boulders of carbonate rock (density of *ca* 2600 to 2700 kg m^{-3}) piggyback along the top of flow. This phenomenon, also typical of plug-like flows composed of sediment and devoid of snow (= debris flows), has been discussed for decades (see, e.g. Rodine & Johnson, 1976; Coussot & Piau, 1994; Coussot & Meunier, 1996; Iverson & Vallance, 2001; Legros, 2002; Phillips, 2006). In a thought experiment, a boulder could be placed onto a static layer of wet, granular snow: the boulder will sink into the snow by mechanical compaction, but it will not sink immediately to ground. This is because of two effects: (i) the compacted snow grains provide a grain-supported fabric, sustaining weight; and (ii) because of pressure solution, at least part of the boulder weight will be sustained by hydrostatic pressure in pores between snow grains.

The validity of this 'static' concept is supported by the fact that the vertical distribution of 6511-boulders and underlying, pure avalanche snow remained the same during the entire phase of snowmelt. As described, boulders up to about 3 m in size readily melted out from layer B, and then remained on the very surface of the downmelting, pure avalanche snow underneath. For avalanche movement as a layered plug-like flow – at least when the avalanche was developed fully (cf. Iverson & Vallance, 2001) – it is assumed that the weight of both the boulder plus underlying snow was supported within a strongly sheared lower zone of the avalanche. In this layer, snow grains may be organized into collectives vertically separated from each other by discrete slide planes. In addition, in a sheared granular medium with interstitial fluid, pore pressures higher than static equilibrium pressure can reduce grain-contact stresses (Iverson, 1997; Major & Iverson, 1999; Iverson & Vallance, 2001). For wet-snow avalanches, Sovilla *et al.* (2010) suggested that quasi-cyclic pressure fluctuations measured at a vertical obstacle result from buildup and disintegration of snow clusters providing 'force chains'. The building blocks (individual snow grains and/or collectives thereof) that may support force chains are not fully clear at present (cf. Sovilla *et al.*, 2010). Force chains of snow-grain collectives perhaps may also vertically support cobbles to boulders during avalanche flow. This does not exclude the additional action of other mechanisms, such as supra-hydrostatic pore fluid pressure.

A two-layer stratigraphy is a widespread feature of scree-laden snow-avalanche deposits (cf. Ballantyne, 1987; Luckman, 1988; Bell *et al.*, 1990; Jomelli & Bertran, 2001). In most cases, however, because of observation well after the event, it is not clear whether an avalanche deposit was triggered by rockfall or by instability of snow cover, or whether the vertical layering reflects a stacking of successive avalanches. Primary two-layer stratifications formed during single avalanche events are indicated by direct field observations on scree-laden, wet-snow avalanches triggered by instability of the snow cover (Lorenzi, 2012). Jomelli & Bertran (2001) implicitly suggested that the surficial layer of 'scree + snow' forms during halting of the avalanche. This may apply to avalanches rich in material ripped up from the substrate (for example, scree, soil and shrubs) in the starting zone. During halting of a ground avalanche, thrust surfaces propagating upslope and up-section can telescope material from the tailing part of the avalanche onto the top of the already halted portion of the avalanche. In the early morning of 23 March 2012, at a location 30 km west of Innsbruck, a rockfall 76 000 m^3 in volume onto snow-covered talus forced off a scree-laden snow avalanche (currently subject to investigation). Although the volume and details of the downslope trajectory of this avalanche differ from that described herein, the deposit also consisted of: (i) a thicker, lower layer of pure granular snow with slide planes; and (ii) an upper layer containing unsorted clastic material from clay-sized grains to boulders up to *ca* 6 m in width. These observations underscore that 'two-layer' flow probably is a widespread feature of avalanches triggered by rockfall loading.

Parameter comparison

In view of its runout towards the end of the scree slope and its path length, the rockfall-induced snow avalanche classifies as a size 3 or medium-scale avalanche, respectively (see European Avalanche Warning Services – www.avalanches.org). Rockfall-triggered, heavily scree-laden avalanches are not included, neither in models of 'rockfall' runout, nor of snow-avalanche movement. Models of rockfall runout treat settings wherein rock particles fall down more-or-less freely from the start (e.g. Meißl, 1998; Bourrier *et al.*, 2009; De Blasio & Saeter, 2009). In this case, the geometrical parameterization of an event is relatively straightforward (Evans & Hungr, 1993; but see Keylock & Domaas, 1999). For the 6511-event, of the diverse geometrical parameters to characterize rockfalls, the best determinable one is the shadow angle (see Evans & Hungr, 1993; Dorren, 2003), with a value of 30° (angle alpha in inset in Fig. 2B). This angle is well within a range of shadow angles of 21° to 42° reported for rockfalls on other scree slopes (cf. Evans & Hungr, 1993; Meißl, 1998; Guzzetti *et al.*, 2003; Copons *et al.*, 2009; Stock *et al.*, 2012).

The fahrböschung of a rockfall or rock avalanche is the angle from the upper end of the detachment scar to the downslope terminus of the resulting event deposit (angle beta in inset in Fig. 2B; e.g. Scheidegger, 1973). With the reservation that there are fundamental mechanical differences between rockfalls and rock avalanches (see e.g. Evans & Hungr, 1993; McSaveney & Davies, 2002; Evans *et al.*, 2006; Imre *et al.*, 2010), the fahrböschung of 54° of the 6511-event may be compared with other rockfalls. In the Northern Calcareous Alps (Eastern Alps), the fahrböschung values of 21 rockfalls descended *without* major topographic confinements or obstacles along their path range from 29° to 48·5° (Meißl, 1998, fig. 17). An identical fahrböschung of 54° was determined for a $2{\cdot}19 \times 10^6$ m^3 rock avalanche at El Capitan, Yosemite valley (Stock & Uhrhammer, 2010); this angle is much higher than a 'should-be' fahrböschung of 20° to 23° (or 30°, if the upper limit of 1 standard deviation is taken) according to a linear regression between landslide volume and fahrböschung (see Scheidegger, 1973, fig. 2; Collins & Melosh, 2003, fig. 1). The rock avalanche at El Capitan defaced from the topmost part of the cliff, fell down freely over 650 m in altitude, and then impacted a talus dipping *ca* 20°. The impact of the vertically downfalling rock mass onto a gently dipping surface dissipated most of the kinetic energy; as a result, the rock mass could run out only for a small distance downslope of the impact area (Stock & Uhrhammer, 2010). This highlights the strong control of geometry (such as steepness, continuity or inversion of slope, curvatures, channelling or not, etc.) of the travel path of mass movements on runout (Nicoletti & Sorriso-Valvo, 1991).

The fahrböschung is identical in geometrical definition to the runout angle alpha as used in snow-avalanche research (see, e.g. Lied & Bakkehøi, 1980; Smith & McClung, 1987). Cursory field observations since 2001 indicate that rela-

tively small, 'high-frequency' avalanches with a return period of less than 100 years (cf. Smith & McClung, 1987) are common on Riepen talus. The 30° shadow angle of the 6511-event is close to a mean runout angle of 32·5° deduced by Smith & McClung (1987) for high-frequency, pure-snow avalanches in the Columbia Mountains of Canada. Thus, with respect to its shadow/runout angles, the 6511-event is not exceptional. In summary, it is inferred that the high 54°-fahrböschung of the 6511-event combined with a shadow/runout angle of 30° results from consumption of kinetic energy when the rockmass fragmented downway along the summit gorge. In addition, a relatively small runout of the avalanche probably resulted from the superposed effects of: (i) a stable snow cover before rockfall impact; (ii) the open slope that allowed the avalanche to spread out laterally, so to more effectively dissipate kinetic energy; (iii) the downslope profile of the talus, with a proximal segment (36° to 34° dip) sharply switching to much lower dip at 2285 m a.s.l.; and (iv) the boulders littered in the lower part of the talus that consumed part of the kinetic energy of the avalanche in bypassing.

Grain-size distribution (fraction ≤16 mm)

As mentioned, due to numerous rock showers in the aftermath of the 6511-rockfall, the sediment samples from the apex of Riepen talus (Fig. 12A) could be collected only from 16 September 2011, i.e. more than five months thereafter. It is assumed that the apical sediment reflects the finer-grained fraction of pristine rockfall material derived from Riepenwand, whereas (as observed in the field) coarser-grained rockfall clasts were transported to locations further down on the slope. Conversely, the unsorted scree of clay to boulder particle size of avalanche layer B (Fig. 12B) only reflects rockfall-related fracturation; there was no time and no opportunity for other processes to significantly modify the grain-size distribution of this sediment since its first deposition within the avalanche. In the grain-size fraction ≤16 mm, the scree of both the apex and of layer B are very similar. This is not surprising, because both sediments originated from rockfall and (in the size fraction ≤16 mm) were subject to little, if any, modification since first deposition on the slope. In the samples of the stratified scree slopes, however, the grain-size distribution of the fraction ≤16 mm shows a comparatively large scatter (Fig. 12C). Because the samples for sieving were taken *per stratum* from excavations into scree slopes, this is explained by differences in clast fabric and sorting among strata. The similarity of grain-size distributions ≤16 mm of pristine rockfall materials with the *average* size distribution of the stratified scree slopes is, however, notable; this holds in particular for the similar average content in matrix ≤0·063 mm between 5 wt% and 10 wt%. It can be assumed that a portion of the matrix of scree slopes is produced by processes other than rockfall (see Sanders *et al.*, 2010). If so, the average matrix content of the stratified scree slopes would be expected to differ significantly from that of the pristine rockfall material, which is not the case. It thus seems most parsimonious to conclude that the *average* grain-size distribution and matrix content, in the fraction ≤16 mm, of the stratified scree slopes largely reflect disintegration by rockfall.

As described, subsequent to emplacement, rockfall-derived boulders were observed to further disintegrate. In addition, due to the dense jointing of the metadolostones, with time, older boulders are seen to be surrounded by a litter of cobble-sized to pebble-sized fragments produced by physical weathering while the boulder rests in place. Thus, in particular, the coarse-pebbly to bouldery sediment fraction is subject to post-depositional shift of its grain-size distribution. The SEM inspection of the 6511-matrix suggests that practically all of it was produced by fragmentation during the rockfall. The dolomite particles bounded by rhombohedral surfaces (Fig. 11A and C) may result from fracture along either intercrystalline pores and/or intracrystalline cleavage. The lack of grains ≤0·3 to 0·5 μm in size, as indicated by the Mastersizer measurements (Fig. 13), may be explained by physical processes and/or by dissolution. Because the kinetic energy required for particle fracture increases exponentially with decreasing grain size, the lower comminution limit for most materials is *ca* 1 μm (e.g. Kendall, 1978; An & Sammis, 1994). Ultra-fine mineral particles produced by fracture may store residual strain in the lattice, which renders them 'supersoluble'. The absence of grains ≤0·3 to 0·5 μm thus may reflect a physical comminution limit and/or removal by dissolution.

Rock cliffs are morphologically differentiated by benches, chutes and dihedra, and many show a steeply inclined lower buttress. Most rock masses defaced from cliffs thus are subject to impact and fragmentation during descent,

Table 2. Surface features indicative of scree transport by snow avalanches on talus.

Feature	Interpretation	Remarks, references
Concave slope devoid of chutes, may show steep front and elongated low-dipping distal part ('roadbank') Distal part of slope may show: (i) litters of cobbles to boulders; (ii) longitudinal boulder tongues; (iii) grooves; and (iv) debris tails Debris tails: Ridges parallel to avalanche flow, extend upslope and downslope of boulders on talus surface	Shaping of talus surface by snow avalanches	Debris tails: Some may be erosional, others depositional Rapp (1959, 1960), Gardner (1970), Luckman (1977, 1978, 1992)
Isolated boulders to cobbles perched along slope; boulders to cobbles may be placed in precarious positions	(i) Dampened impact of boulders falling into snow, preventing or limiting downslope transport by rolling and bouncing; and/or (ii) downslope transport by snow avalanche	Rapp (1960), Gardner (1970), Luckman (1977, 1978), Matthews & McCarroll (1994), Decaulne & Saemundsson (2010)
Avalanche impact landforms, scour pits: Downslope-elongate to subcircular depressions down to a few metres in depth, up to a few hundreds of metres in area; may be filled by ponds (tarns)	Erosional features from impact and scouring of snow avalanches; probably produced by successive avalanches	Luckman (1977), Corner (1980), Fitzharris & Owen (1984), Matthews & McCarroll (1994), Smith *et al.* (1994), Owen *et al.* (2006), Johnson & Smith (2010)
Depositional avalanche impact forms, impact tongues: tongue-shaped debris accumulations; oblique to transverse to main avalanche flow direction Some protalus ramparts may (additionally) form by snow-avalanche impact	Depositional features produced by redeposition of scree by avalanche erosion and impact	Corner (1980), Matthews *et al.* (2011)
Boulders with cobbles to pebbles placed on top	Deposition of clasts on boulder top by melting of avalanche snow	Luckman (1988)
Lichenized boulders with bare, unlichenized patches	Bare patches result from lack of lichenization due to placement of clast on top of the boulder. Clast was later purportedly removed by a snow avalanche	In view of time needed for lichenization, this feature requires at least a few decades to develop Ward (1985)
Boulder holes	Negative imprints left by boulders plucked out of place bypassing snow avalanche	Ward (1985)
(i) Impact and scratch marks on boulders in the distal part of slope, and beyond reach of rockfall impacts. (ii) Polished and striated patches on lichenized cobbles to boulders	(i) Marks generated by stones embedded in overriding snow avalanche. (ii) Abrasion of clast surface by snow avalanche laden with stones and soil	Ward (1985), Braunhofer (2011)

before hitting a scree slope. Fragmentation during fall and upon impact on the scree slope results in generation of dust of clay-grade to silt-grade material. Depending on cliff morphology and the locus of defacement, rockfalls may even be largely turned to dust. For instance, on 12 October 2007 on Einserkofel (2698 m a.s.l.; The Dolomites, Italy), a rockfall of an estimated volume of 60 000 m^3 defaced between 2400 m and 2600 m a.s.l. within a deep chute. Eyewitness reports and videos showed that the rock mass first crunched down the chute, then fell down freely, it next impacted the buttress of the cliff, and finally poured out onto the scree slope. As a result of this trajectory a large part, perhaps even most, of the falling rock mass turned to dust. Under calm fair weather, a huge cloud of rockfall-generated dust slowly fell out in a drape that, near the rockfall impact, was up to *ca* 20 cm in thickness. Conversely, on the scree slope, comparatively little pebble-sized to boulder-sized rockfall material had accumulated; the impression was that much or most of the fallen rock volume was fragmented to dust. Unfortunately, this rockfall was not subject to more detailed geological investigation. As mentioned, Wieczorek *et al.* (2000) described two large rockfalls associated with airblasts. In the airblast damage zone, grain-size analyses of the settled dust indicate a relative content of matrix (material ≤0·063 mm in grain size, as understood herein) of *ca* 5 to 25 wt%. The rocks in that case were granodiorite and tonalite. The original dust cloud, however, was richer in fine-grained material, because a layer of dust up to a few millimetres thick fell out over an area extending for more than a kilometre beyond the damage zone (see Wieczorek *et al.*, 2000). Overall, it seems that rockfalls with a volume of more than a few tens of cubic metres are associated with sizeable dust clouds, irrespective of rock type (see Gordon *et al.*, 1978; Wieczorek *et al.*, 2000, 2008; Guzzetti *et al.*, 2003; Krähenbühl, 2006; Graf & Tobler, 2008). Rockfall, however, is not the only process to contribute fine-grained matrix to talus. For instance, biological infestation of rock (talus clasts and cliff surfaces) can produce fine-grained material (Moses & Smith, 1993) by loosening the mineral grain structure via physico-chemical attack (Sand, 1997; Hoppert *et al.*, 2004; Horath *et al.*, 2006;

Table 3. Possible geological features of scree deposition associated with snow avalanches.

Location, feature	Interpretation	Remarks, references
1: Proximal, steep-dipping part of slope succession: (A) Isolated boulders, or clusters of boulders, intercalated in succession of stratified scree mainly of poorly to well-sorted pebbles (B) Isolated boulders associated with upslope debris horns	(A) (i) Downslope transport in snow avalanche; or (ii) dampened impact of boulder falling into snow cover (without avalanche); or (iii) debris flow or slush flow onto snow cover (B) (i) Boulders trap lithoclasts transported downslope in snow avalanche; or (ii) hold back lithoclasts transported downslope by other processes (grain flow, rolling, bouncing)	Whitehouse & McSaveney (1983), Ward (1985), Sanders *et al.* (2009)
2: Distal, low-dipping part of slope succession: Intervals, up to a few metres thick, with: (a) indistinct stratification; (b) openwork clast fabric, locally with interstices (partly) filled by internal sediment; larger clast interstices may contain stratified waterlain infill; (c) chunks of ripped-up soil; (d) 'rolling boulder fabric' (arrays of isolated boulders embedded subparallel to stratification)	In interpretation, all of these features should be applied in combination	Blikra & Selvik (1998), Blikra & Nemec (1998) Except perhaps for very large and heavily scree-laden snow avalanches, deposition of a geological interval (more than one to two clasts in thickness) may require repeated avalanche descends over some interval of time. Facies may be mixed with talus facies of other origins

Weber *et al.*, 2010). The potential interactions of epilithic and endolithic rock colonization (e.g. Chen *et al.*, 2000; Etienne, 2002; Pohl & Schneider, 2002) with microgelivation (cf. Matsuoka, 2001; Matsuoka & Murton, 2008) in producing fine-grained sediment is hardly explored. In a study of late-glacial to Holocene talus development on Mynydd Du (Wales) and associated retreat of cliffs composed of marls, sandstones and conglomerates, Curry & Morris (2004) concluded that *ca* 27% of cliff retreat may be attributable to microgelivation. These authors did not refer to the type and pathways of sediment from microgelivation. In cold-arid environments, fine-grained sediment is produced by thermal stress fatigue at the mineral grain scale by cyclic heating and cooling (Hall, 1999; Hall & André, 2003). In brief, while rockfall-related fragmentation can produce a major share of the matrix of talus, depending on rock type and climate, other processes might contribute to or even prevail in matrix generation.

Preservation potential

The observations up to autumn 2012 record the beginning of redeposition and overprint of the 6511-deposit (Fig. 14). Satellite and laser scan images prior to the 6511-event (Fig. 2), and field data from years before 2011 (Kilian, 2008; Reichhalter, 2009), indicate that the pattern of surface run-off on the scree slope is similar before and after the event. This drainage pattern is dictated by the boundary between the toe of the rock cliff and the scree slope. The preservation potential of the estimated 5 to 6 m of event-related aggradation of the talus apex seems to be low; this is suggested by the significant, and ongoing, redeposition of apex material by debris flows further downslope within about 18 months after the event (Fig. 14E and F). Provided that no major depositional or erosional event will affect Riepen talus in the near future, further changes will include: (i) degradation of the 6511-apex and redeposition of apical material in the proximal part of slope; (ii) illuviation of fallen out dust and of layer-B matrix into pore space; (iii) downslope particle creep of rockfall-derived pebbles to boulders in the proximal slope, accompanied by mixing with older scree and with clasts from future rock showers; (iv) partial disintegration of 6511-boulders to cobbles into clasts mainly of cobble to pebble size; and (v) weathering and lichenization of 6511-clast surfaces. The fresh rockfall clasts will become fully colonized and infested by epilithic and endolithic lichens, fungi, cyanobacteria and other bacteria within some 100 to 150 years (cf. Chen *et al.*, 2000; Pohl & Schneider, 2002; Hoppert *et al.*, 2004).

On talus surfaces, a spectrum of features indicates scree transport by snow avalanches (Table 2), but the record is highly variable in clarity and scale (cf. Ward, 1985): slopes passed every year, or nearly so, by at least one large snow avalanche may be shaped into avalanche roadbanks (e.g. Rapp, 1959, 1960; Luckman, 1977; Jomelli & Bertran, 2001); slopes subject to more-or-less regular avalanching, but also to significant influence, for instance of debris flows and ephemeral water run-off, show surface characteristics transitional between 'end-member types' (Jomelli & Bertran, 2001); finally, slopes passed relatively rarely by avalanches may provide only a more subtle record (Ward, 1985; Braunhofer, 2011). For the geologist dealing with vertical sections through talus successions, the question is which surface feature can enter, and in what form, into the final sedimentary record. The geological preservation potential of snow-avalanche transport is limited (Table 3). For instance, in the proximal, steep-dipping part of fossil talus, isolated boulders may indicate snow-avalanche transport. Boulders high up on the steep part of slope, however, can also be emplaced by: (i) fall into snow cover quenching further downslope bouncing and rolling; and/or (ii) low fall distance or toppling from the basal part of a cliff. For the distal, low-dipping part of slope, intervals of unstratified to faintly stratified openwork fabrics of extremely poorly sorted pebbles to boulders, with partial geopetal infillings of matrix, are considered characteristic of repeated transport by snow avalanches (Blikra & Selvik, 1998; Table 3). To accumulate a finite interval of such deposits may require repeated scree-laden snow avalanching, combined with lack of redeposition of sediment after snowmelt. Apart from snowmelt, rain and ephemeral surface run-off are also effective in illuviating matrix into interstitial pore space. In fossil carbonate-lithic talus successions of the Eastern Alps, to date it has not been possible to unambiguously identify a sedimentary facies accumulated only from snow-avalanche transport; this may be related to post-avalanche overprint, and/or to other processes that may produce similar results, rather than to the rarity of avalanche transport (Sanders *et al.*, 2009). In the distal part of fossil talus, perhaps much of the scree was originally carried down by snow avalanches.

Clear-cut identification of overprint of the original, avalanche-deposited sediment and distinction of avalanche-deposited scree from other facies, however, remains a challenge.

ACKNOWLEDGEMENTS

The paper benefited from the comments of two anonymous reviewers. Captain Jochen Tiefengraber and Dr Michael Said, Christophorus Helicopter Ambulance, are thanked for providing photographs of the 6511-rockfall, and for an excerpt of the flight protocol of 6 May 2011. Heinz Moser, Axams, is equally thanked for mailing his ground-based photographs taken on the day of the rockfall event. Helmut Hausmann, Zentralanstalt für Meteorologie und Geodynamik, Vienna, kindly provided the seismograms to determine event time. Reinhard Starnberger (Institute of Geology) is also thanked for an introduction to and discussion of Mastersizer 2000® measurements, to Andreas Saxer (Institute of Material Technology) for advice on the low-vacuum SEM. Rudolf Sailer (Institute of Geography) and Thomas Sausgruber (Austrian Service for Torrent and Avalanche Control) are thanked for discussions of avalanche dynamics. Thomas Sausgruber also provided a volume estimate of a similar rockfall onto snow on 23 March 2012. Finally, Lorenz Keim is thanked for initially guiding the first author's attention to the phenomenon of dust generation during rockfalls.

REFERENCES

Ampferer, O. (1907) Über Gehängebreccien der nördlichen Kalkalpen. *Jahrbuch der geologischen Reichsanstalt*, **57**, 727–752.

Ampferer, O. (1943) Die Schlußvereisung der Kalkkögel bei Innsbruck. *Sitzungsberichte der Akademie der Wissenschaften in Wien*, **152**, 255–274.

An, L.-J. and **Sammis, C.G.** (1994) Particle size distribution of cataclastic fault materials from southern California: a 3-D study. *Pure Appl. Geophys.*, **143**, 203–227.

André, M.-F. (1990) Geomorphic impact of spring avalanches in Northwest Spitsbergen (79° N). *Permafrost Periglac. Process.*, **1**, 97–110.

Ballantyne, C.K. (1987) Some observations on the morphology and sedimentology of two active protalus ramparts, Lyngen, northern Norway. *Arctic Alpine Res.*, **19**, 167–174.

Bell, I., **Gardner, J.** and **de Scally, F.** (1990) An estimate of snow avalanche debris transport, Kaghan valley, Himalaya, Pakistan. *Arctic Alpine Res.*, **22**, 317–321.

Bertran, P. and **Texier, J.-P.** (1999) Facies and microfacies of slope deposits. *Catena*, **35**, 99–121.

Blikra, L.H. and **Nemec, W.** (1998) Postglacial colluvium in western Norway: depositional processes, facies and palaeoclimatic record. *Sedimentology*, **45**, 909–959.

Blikra, L. and **Selvik, S.F.** (1998) Climatic signals recorded in snow avalanche-dominated colluvium in western Norway: depositional facies successions and pollen records. *Holocene*, **8**, 631–658.

Bourrier, F., **Dorren, L.**, **Nicot, F.**, **Berger, F.** and **Darve, F.** (2009) Toward objective rockfall trajectory simulation using a stochastic impact model. *Geomorphology*, **110**, 68–79.

Brandner, R., **Resch, W.** and **Reiter, F**. (2003) Das Brennermesozoikum. Sedimentäre Faziesentwicklungen in metamorphen Gesteinen und tektonische Konsequenzen. Arbeitstagung der Geologischen Bundesanstalt, Blatt 148 Brenner. Geological Survey of Austria, Vienna, 95–98.

Braunhofer, D. (2011) Erscheinungen von Schneelawinen-Erosion auf der Innsbrucker Nordkette. Unpubl. B.Sc. thesis, University of Innsbruck, 29 pp.

Brückl, E., **Brunner, F.K.**, **Gerber, E.** and **Scheidegger, A.E.** (1974) Morphometrie einer Schutthalde. *Mitteilungen der österreichischen geographischen Gesellschaft in Wien*, **116**, 79–96.

Brugnot, G. and **Pochat, R.** (1981) Numerical simulation study of snow avalanches. *J. Glaciol.*, **27**, 77–88.

Brun, E. and **Rey, L**. (1987) Field study on snow mechanical properties with special regard to liquid water content. In: *Avalanche Formation, Movement and Effects* (Eds B. Salm and H. Gubler), *Int. Assoc. Hydrol. Sci. Publ.*, **162**, 183–193.

Buser, O. and **Bartelt, P.** (2011) Dispersive pressure and density variations in snow avalanches. *J. Glaciol.*, **57**, 857–860.

Chen, J., **Blume, H.-P.** and **Beyer, L.** (2000) Weathering of rocks induced by lichen colonization – a review. *Catena*, **39**, 121–146.

Christen, M., **Kowalski, J.** and **Bartelt, P.** (2010) RAMMS: numerical simulation of dense snow avalanches in three-dimensional terrain. *Cold Reg. Sci. Technol.*, **63**, 1–14.

Collins, G. S. and **Melosh, H. J**. (2003) Acoustic fluidization and the extraordinary mobility of sturzstroms. *J. Geophys. Res.*, **108**, B10, 2473. doi:10.1029/2003JB002465.

Copons, R., **Vilaplana, J.M.** and **Linares, R.** (2009) Rockfall travel distance analysis by using empirical models (Solá d'Andorra la Vella, Central Pyrenees). *Nat. Hazards Earth System Sci.*, **9**, 2107–2118.

Corner, G.D. (1980) Avalanche impact landforms in Troms, north Norway. *Geogr. Ann.*, **62A**, 1–10.

Coussot, P. and **Meunier, M.** (1996) Recognition, classification and mechanical description of debris flows. *Earth Sci. Rev.*, **40**, 209–227.

Coussot, P. and **Piau, J.-M**. (1994) Some considerations on debris flow rheology. In: *Dynamics and Geomorphology of Mountain Rivers* (Eds P. Ergenzinger and K.-H. Schmidt), *Lect. Notes Earth Sci.*, **52**, 315–326. Springer, Berlin.

Crosta, G.B., **Frattini, P.** and **Fusi, N.** (2007) Fragmentation in the Val Pola rock avalanche, Italian Alps. *J. Geophys. Res.*, **112**, F01006. doi:10.1029/2005JF000455.

Cruden, D.M. and **Hu, X.-Q.** (1999) The shapes of some mountain peaks in the Canadian Rockies. *Earth Surf. Proc. Land.*, **24**, 1229–1241.

Curry, A.M. and **Morris, C.J.** (2004) Lateglacial and Holocene talus slope development and rockwall retreat on Mynydd Du, UK. *Geomorphology*, **58**, 85–106.

Daerr, A. and **Douady, S.** (1999) Two types of avalanche behaviour in granular media. *Nature*, **399**, 241–243.

Davies, M.C.R., **Hamza, O.** and **Harris, C.** (2001) The effect of rise in mean annual temperature on the stability of rock slopes containing ice-filled discontinuities. *Permafrost Periglac. Process.*, **12**, 137–144.

De Blasio, F.V. and **Saeter, M.-B.** (2009) Small-scale experimental simulation of talus evolution. *Earth Surf. Proc. Land.*, **34**, 1685–1692.

De Scally, F.A. and **Owens, I.F.** (2005) Depositional processes and particle characteristics on fans in the Southern Alps, New Zealand. *Geomorphology*, **69**, 46–56.

De Toni, S. and **Scotton, P.** (2005) Two-dimensional mathematical and numerical model for the dynamics of granular avalanches. *Cold Reg. Sci. Technol.*, **43**, 36–48.

Decaulne, A. and **Saemundsson, T.** (2006) Geomorphic evidence for present-day snow-avalanche and debris-flow impact in Icelandic Westfjords. *Geomorphology*, **80**, 80–93.

Decaulne, A. and **Saemundsson, P.** (2010) Distribution and frequency of snow-avalanche debris transfer in the distal part of colluvial cones in Central North Iceland. *Geogr. Ann.*, **92A**, 177–187.

Dent, J.D. and **Lang, T.E.** (1982) Experiments on the mechanics of flowing snow. *Cold Reg. Sci. Technol.*, **5**, 243–248.

Dietrich, H. (1983) Zur Petrologie und Metamorphose des Brennermesozoikums (Stubaier Alpen, Tirol). *Tschermaks mineralogische und petrographische Mitteilungen*, **31**, 235–257.

Donofrio, D.A. (2008) Kurzmitteilung zu Conodonten, Echinodermen- und Fischresten aus dem Brenner-Mesozoikum (Kalkkögelgruppe SW Innsbruck, Tirol) und deren Paläotemperaturen. *Geo.Alp*, **5**, 83–95.

Dorren, L.K.A. (2003) A review of rockfall mechanisms and modelling approaches. *Prog. Phys. Geogr.*, **27**, 69–87.

Etienne, S. (2002) The role of biological weathering in periglacial areas: a study of weathering rinds in south Iceland. *Geomorphology*, **47**, 75–86.

Evans, S.G. and **Hungr, O.** (1993) The assessment of rockfall hazard at the base of talus slopes. *Can. Geotech. J.*, **30**, 620–636.

Evans, S. G., **Scarascia Mugnozza, G.**, **Strom, A. l.**, **Hermanns, R. L.**, **Ischuk, A.** and **Vinnichenko, S**. (2006) Landslides from massive rock slope failure and associated phenomena. In: *Landslides from Massive Rock Slope Failure* (Eds S.G. Evans, G. Scarascia Mugnozza, A. Strom and R. L. Hermanns), NATO Sci. Ser., pp. 3–52. Springer, Dordrecht.

Fitzharris, B.B. and **Owen, I.F.** (1984) Avalanche tarns. *J. Glaciol.*, **30**, 308–312.

Folk, R.L. (1974) The natural history of crystalline calcium carbonate: effect of magnesium content and salinity. *J. Sed. Petrol.*, **44**, 40–53.

Frank, W., **Hoinkes, G.**, **Purtscheller, F.** and **Thöni, M.** (1987) The Austroalpine Unit west of the Hohe Tauern: the Oetztal-Stubai Complex as an example for the Eoalpine metamorphic evolution. In: *Geodynamics of the Eastern Alps* (Eds H.W. Flügel and P. Faupl), pp. 179–225. Franz Deuticke, Vienna.

French, H.M. (2007) *The Periglacial Environment*. John Wiley and Sons Ltd.Chichester, 458 pp.

Fügenschuh, B., **Seward, D.** and **Mancktelow, N.** (1997) Exhumation in a convergent orogen: the western Tauern window. *Terra Nova*, **9**, 213–217.

Fügenschuh, B., **Mancktelow, N.** and **Seward, D.** (2000) Cretaceous to Neogene cooling and exhumation history of the Oetztal-Stubai basement complex, eastern Alps: a structural and fission track study. *Tectonics*, **19**, 905–918.

Fuhrmann, S. (2012) Der Felssturz vom 6. 5. 2011 an der Riepenwand: Volumen und Charakteristika. Unpubl. B.Sc. thesis, University of Innsbruck, 37 pp.

Gardner, J. (1970) Geomorphic significance of avalanches in the Lake Louise area, Alberta, Canada. *Arctic Alpine Res.*, **2**, 135–144.

Geyssant, J. (1973) Stratigraphische und tektonische Studien in der Kalkkögelgruppe bei Innsbruck in Tirol. *Verhandlungen der Geologischen Bundesanstalt*, **3**, 377–396.

Gordon, J.E., **Birnie, R.V.** and **Timmis, R.** (1978) A major rockfall and debris slide on the Lyell glacier. *Arctic Alpine Res.*, **10**, 49–60.

Graf, K. and **Tobler, D.** (2008) Der Felssturz am "Hellhore" in Kandersteg vom 16. August 2008. *Bulletin für Angewandte Geologie*, **13**, 97–106.

Gruber, S. and **Haeberli, W**. (2007) Permafrost in steep bedrock slopes and its temperature-related destabilization following climate change. *J. Geophys. Res.*, **112**, F02S18. doi:10.1029/2006JF000547.

Gruber, S., **Hoelzle, M.** and **Haeberli, W.** (2004) Rock-wall temperatures in the Alps: modelling their topographic distribution and regional differences. *Permafrost Periglac. Process.*, **15**, 299–307.

Guzzetti, F., **Reichenbach, P.** and **Wieczorek, G.F.** (2003) Rockfall hazard and risk assessment in the Yosemite valley, California, USA. *Nat. Hazards Earth Syst. Sci.*, **3**, 491–503.

Hall, K. (1999) The role of thermal stress fatigue in the breakdown of rock in cold regions. *Geomorphology*, **31**, 47–63.

Hall, K. and **André, M.-F.** (2003) Rock thermal data at the grain scale: applicability to granular disintegration in cold environments. *Earth Surf. Proc. Land.*, **28**, 823–836.

Heckmann, T., **Bimböse, M.**, **Krautblatter, M.**, **Haas, F.**, **Becht, M.** and **Morche, D.** (2012) From geotechnical analysis to quantification and modelling using LIDAR data: a study on rockfall in the Reintal catchment, Bavarian Alps, Germany. *Earth Surf. Proc. Land.*, **37**, 119–133.

Hinchliffe, S., **Ballantyne, C.K.** and **Walden, J.** (1998) The structure and sedimentology of relict talus, Trotternish, Northern Skye, Scotland. *Earth Surf. Proc. Land.*, **23**, 545–560.

Hoppert, M., **Flies, C.**, **Pohl, W.**, **Günzl, B.** and **Schneider, J.** (2004) Colonization strategies of lithobiontic microorganisms on carbonate rocks. *Environ. Geol.*, **46**, 421–428.

Horath, T., **Neu, T.R.** and **Bachofen, R.** (2006) An endolithic microbial community in dolomite rock in central Switzerland: characterization by reflection spectroscopy, pigment analyses, scanning electron microscopy, and laser scanning microscopy. *Microbiol. Ecol.*, **51**, 353–364.

Imre, B., **Laue, J.** and **Springmann, S.M.** (2010) Fractal fragmentation of rocks within sturzstroms: insight derived from physical experiments within the ETH geotechnical drum centrifuge. *Granular Matter*, **12**, 267–285.

Issler, D., **Errera, A.**, **Priano, S.**, **Gubler, H.**, **Teufen, B.** and **Krummenacher, B.** (2008) Inferences on flow mechanisms from snow avalanche deposits. *Ann. Glaciol.*, **49**, 187–192.

Iverson, R.M. (1997) The physics of debris flows. *Rev. Geophys.*, **35**, 245–296.

Iverson, R.M. and **Vallance, J.W.** (2001) New views of granular mass flows. *Geology*, **29**, 115–118.

Ivy-Ochs, S., **Kerschner, H.**, **Kubik, P.W.** and **Schlüchter, C.** (2006) Glacier response in the European Alps to Heinrich event I cooling: the Gschnitz stadial. *J. Quatern. Sci.*, **21**, 115–130.

Ivy-Ochs, S., **Kerschner, H.**, **Maisch, M.**, **Christl, M.**, **Kubik, P.W.** and **Schlüchter, C.** (2009) Latest Pleistocene and Holocene glacier variations in the European Alps. *Quatern. Sci. Rev.*, **28**, 2137–2149.

Johnson, A.L. and **Smith, D.J.** (2010) Geomorphology of snow avalanche impact landforms in the southern Canadian Cordillera. *Can. Geogr.*, **54**, 87–103.

Jomelli, V. and **Bertran, P.** (2001) Wet snow avalanche deposits in the French Alps: structure and sedimentology. *Geogr. Ann.*, **83A**, 15–28.

Jomelli, V. and **Francou, B.** (2000) Comparing the characteristics of rockfall talus and snow avalanche landforms in an Alpine environment using a new methodological approach: Massif des Ecrins, French Alps. *Geomorphology*, **35**, 181–192.

Kendall, K. (1978) The impossibility of comminuting small particles. *Nature*, **272**, 710–711.

Kern, M., **Tiefenbacher, F.** and **McElwaine, J.** (2004) The rheology of snow in large chute flows. *Cold Reg. Sci. Technol.*, **39**, 181–192.

Kern, M., **Bartelt, P.**, **Sovilla, B.** and **Buser, O.** (2009) Measured shear rates in large dry and wet snow avalanches. *J. Glaciol.*, **55**, 327–338.

Kerschner, H. (1986) Zum Sendersstadium im Spätglazial der nördlichen Stubaier Alpen, Tirol. *Zeitschrift für Geomorphologie, Neue Folge*, Supplement-Band 61, 65–76. Gebrüder Borntraeger, Berlin, Stuttgart.

Keylock, C. and **Domaas, U.** (1999) Evaluation of topographic models of rockfall travel distance for use in hazard applications. *Arct. Antarct. Alpine Res.*, **31**, 312–320.

Kilian, S. (2008) Untersuchung der feinkörnigen Matrix in aktiven, felssturzdominierten Talus-Hängen. Unpubl. B.Sc. thesis, University of Innsbruck, 42 pp.

Kneisel, C. (2010) The nature and dynamics of frozen ground in alpine and subarctic periglacial environments. *Holocene*, **20**, 423–445.

Krähenbühl, R. (2004) Temperatur und Kluftwasser als Ursachen von Felssturz. *Bulletin für angewandte Geologie*, **9**1, 19–35.

Krähenbühl, R. (2006) Der Felssturz, der sich auf die Stunde genau ankündigte. *Bulletin für angewandte Geologie*, **11**, 49–63.

Ladurner, J. (1932) Die Quartärablagerungen des Sellrain (Stubaier Alpen). *Jahrbuch der geologischen Bundesanstalt*, **82**, 397–427.

Lambiel, C. and **Pieracci, K.** (2008) Permafrost distribution in talus slopes located within the Alpine periglacial belt, Swiss Alps. *Permafrost Periglac. Process.*, **19**, 293–304.

Legros, F. (2002) Can dispersive pressure cause inverse grading in grain flows? *J. Sed. Res.*, **72**, 166–170.

Lied, K. and **Bakkehøi, S.** (1980) Empirical calculations of snow-avalanche run-out distance based on topographic parameters. *J. Glaciol.*, **26**, 165–178.

Lorenzi, S. (2012) Grundlawinen im Spätwinter 2012, Nordkette bei Innsbruck. Merkmale und Erosionserscheinungen. Unpubl. B.Sc. thesis, University of Innsbruck, 32 pp.

Luckman, B.H. (1977) The geomorphic activity of snow avalanches. *Geogr. Ann.*, **59A**, 31–48.

Luckman, B.H. (1978) Geomorphic work of snow avalanches in the Canadian Rocky Mountains. *Arctic Alpine Res.*, **10**, 261–276.

Luckman, B.H. (1988) Debris accumulation patterns on talus slopes in Surprise Valley, Alberta. *Géog. Phys. Quatern.*, **42**, 247–278.

Luckman, B.H. (1992) Debris flows and snow avalanche landforms in the Lairig Ghru, Cairngorm Mountains, Scotland. *Geogr. Ann. Series A Phys. Geogr.*, **74**, 109–121.

Major, J.J. and **Iverson, R.M.** (1999) Debris-flow deposition – effects of pore-fluid pressure and friction concentrated at flow margins. *Geol. Soc. Am. Bull.*, **111**, 1424–1434.

Matsuoka, N. (2001) Microgelivation versus macrogelivation: towards bridging the gap between laboratory and field frost weathering. *Permafrost Periglac. Process.*, **12**, 299–313.

Matsuoka, N. and **Murton, J.** (2008) Frost weathering: recent advances and future directions. *Permafrost Periglac. Process.*, **19**, 195–210.

Matsuoka, N. and **Sakai, H.** (1999) Rockfall activity from an alpine cliff during thawing periods. *Geomorphology*, **28**, 309–328.

Matthews, J.A. and **McCarroll, D.** (1994) Snow-avalanche impact landforms in Breheimen, southern Norway: origin, age, and paleoclimatic implications. *Arctic Alpine Res.*, **26**, 103–115.

Matthews, J.A., **Shakesby, R.A.**, **Owen, G.** and **Vater, A.E.** (2011) Pronival rampart formation in relation to snow-avalanche activity and Schmidt-hammer exposure-age dating (SHD): three case studies from southern Norway. *Geomorphology*, **130**, 280–288.

McSaveney, M. J. and **Davies, T. R. H**. (2002) Rapid rock-mass flow with dynamic fragmentation: inferences from the morphology and internal structure of rockslides and rock avalanches. In: *Landslides from Massive Rock Slope Failure* (Eds S. G. Evans, G. Scarascia Mugnozza, A. Strom and R. L. Hermanns), pp. 285–304. NATO Science Series,, Springer, Dordrecht.

Meißl, G. (1998) Modellierung der Reichweite von Felsstürzen. Fallbeispiele zur GIS-gestützten Gefahrenbeurteilung aus dem Bayerischen und Tiroler Alpenraum. *Innsbrucker Geographische Studien*, **28**, 1–249.

Morrissey, M. M., **Savage, W. Z.** and **Wieczorek, G. F**. (1999) Air blasts generated by rockfall impacts: analysis of the 1996 Happy Isles event in Yosemite National Park. *J. Geophys. Res.*, **104**, B10, 23189–23198.

Moses, C.A. and **Smith, B.J.** (1993) A note on the role of the lichen *Collema auriforma* in solution basin development on a carboniferous limestone substrate. *Earth Surf. Proc. Land.*, **18**, 363–368.

Nemec, W. and **Kazanci, N.** (1999) Quaternary colluvium in west-central Anatolia: sedimentary facies and paleoclimatic significance. *Sedimentology*, **46**, 139–170.

Nicoletti, P.G. and **Sorriso-Valvo, M.** (1991) Geomorphic controls of the shape and mobility of rock avalanches. *Geol. Soc. Am. Bull.*, **103**, 1365–1373.

Nötzli, J. and **Gruber, S.** (2005) Alpiner Permafrost – ein Überblick. *Jahrbuch des Vereins zum Schutz der Bergwelt*, **70**, 111–121.

Owen, G., **Matthews, J.A.**, **Shakesby, R.A.** and **He, X.** (2006) Snow-avalanche impact landforms, deposits and effects at Urdvatnet, southern Norway: implications for avalanche style and process. *Geogr. Ann.*, **88A**, 295–307.

Phillips, E. (2006) Micromorphology of a debris flow deposit: evidence of basal shearing, hydrofracturing, liquefaction and rotational deformation during emplacement. *Quatern. Sci. Rev.*, **25**, 720–738.

Pohl, W. and **Schneider, J**. (2002) Impact of endolithic biofilms on carbonate rock surfaces. In: *Natural Stone,*

Weathering Phenomena, Conservation Strategies and Case Studies (Eds S. Siegesmund, T. Weiss and A. Vollbrecht), *Geol. Soc. London Spec. Publ.*, **205**, 177–194.

Pudasaini, S.P. and **Hutter, K.** (2007) *Avalanche Dynamics. Dynamics of Rapid Flows of Dense Granular Avalanches*. Springer, Berlin, 602 pp.

Rajchenbach, J. (2002) The growth of grain avalanches. *Phys. A*, **314**, 304–309.

Rapp, A. (1959) Avalanche boulder tongues in Lappland. *Geogr. Ann.*, **41**, 34–48.

Rapp, A. (1960) Recent development of mountain slopes in Kärkevagge and surroundings, Northern Scandinavia. *Geogr. Ann.*, **42**, 65–200.

Ravanel, L., **Allignol, F.**, **Deline, P.**, **Gruber, S.** and **Ravello, M.** (2010) Rock falls in the Mont Blanc Massif in 2007 and 2008. *Landslides*, **7**,493–501.

Reichhalter, F. (2009) Untersuchung der feinkörnigen Matrix in aktiven, felssturzdominierten Talus-Hängen. Unpubl. B.Sc. thesis, University of Innsbruck, 35 pp.

Reiter, F., **Lenhardt, W.A.** and **Brandner, R.** (2005) Indications for activity of the Brenner normal fault zone (Tyrol, Austria) from seismological and GPS data. *Austrian J. Earth Sci.*, **97**, 16–23.

Rodine, J.D. and **Johnson, A.M.** (1976) The ability of debris, heavily freighted with coarse clastic materials, to flow on gentle slopes. *Sedimentology*, **23**, 213–234.

Sailer, R., **Rammer, L.** and **Sampl, P.** (2002) Recalculation of an artificially released avalanche with SAMOS and validation with measurements from a pulsed Doppler radar. *Nat. Hazards Earth Syst. Sci.*, **2**, 211–216.

Sand, W. (1997) Microbial mechanisms of deterioration of inorganic substrates – a general mechanistic overview. *Int. Biodeterior. Biodegradation*, **40**, 183–190.

Sanders, D. (2011) Hitherto undescribed pattern of rock cliff/talus development: The 'breach concept'. *Geophys. Res. Abstracts*, **13**, EGU2011-1611. EGU General Assembly.

Sanders, D., **Ostermann, M.** and **Kramers, J.** (2009) Quaternary carbonate-rocky talus slope successions (Eastern Alps, Austria): sedimentary facies and facies architecture. *Facies*, **55**, 345–373.

Sanders, D., **Ostermann, M.** and **Kramers, J.** (2010) Meteoric diagenesis of quaternary carbonate-rocky talus slope successions (Northern Calcareous Alps, Austria). *Facies*, **56**, 27–46.

Savage, S. (1979) Gravity flow of cohesionless granular materials in chutes and channels. *J. Fluid Mech.*, **92**, 53–96.

Scheidegger, A.E. (1973) On the predicition of the reach and velocity of catastrophic landslides. *Rock Mechanics*, **5**, 231–236.

Schmid, S.M., **Fügenschuh, B.**, **Kissling, E.** and **Schuster, R.** (2004) Tectonic map and overall architecture of the Alpine orogen. *Eclogae Geol. Helv.*, **97**, 93–117.

Smith, M.J. and **McClung, D.M.** (1987) Characteristics and prediction of high-frequency avalanche runout. *Arctic Alpine Res.*, **29**, 352–357.

Smith, D.J., **McCarthy, D.P.** and **Luckman, B.H.** (1994) Snow-avalanche impact pools in the Canadian Rocky Mountains. *Arctic Alpine Res.*, **26**, 116–127.

Sovilla, B. and **Bartelt, P.** (2002) Observations and modelling of snow avalanche entrainment. *Nat. Hazards Earth Syst. Sci.*, **2**, 169–179.

Sovilla, B., **Sommavilla, F.** and **Tomaselli, A.** (2001) Measurements of mass balanche in dense snow avalanche events. *Ann. Glaciol.*, **32**, 230–236.

Sovilla, B., **Burlando, P.** and **Bartelt, P.** (2006) Field experiments and numerical modeling of mass entrainment in snow avalanches. *J. Geophys. Res.*, **111**, F03007. doi:10.1029/2005JF000391.

Sovilla, B., **Schaer, M.** and **Bartelt, P.** (2008) Impact pressures and flow regimes in dense snow avalanches observed at the Vallée de la Sionne test site. *J. Geophys. Res.*, **113**, F01010. doi:10.1029/2006JF000688.

Sovilla, B., **Kern, M.** and **Schaer, M.** (2010) Slow drag in wet-snow avalanche flow. *J. Glaciol.*, **56**, 587–592.

Sperazza, M., **Moore, J.N.** and **Hendrix, M.S.** (2004) High-resolution particle size analysis of naturally occurring very fine-grained sediment through laser diffractometry. *J. Sed. Res.*, **74**, 736–743.

Stock, G.M. and **Uhrhammer, R.A.** (2010) Catastrophic rock avalanche 3600 years BP from El Capitan, Yosemite Valley, California. *Earth Surf. Proc. Land.*, **35**, 941–951.

Stock, G. M., **Luco, N.**, **Collins, B.**, **Harp, E.**, **Reichenbach, P.** and **Frankel, K. L**. (2012) Quantitative rock-fall hazard and risk assessment for Yosemite Valley, Yosemite National Park, California. Report, Yosemite National Park Service and US Geological Survey, Washington DC, 92 pp.

Thibert, E., **Baroudi, D.**, **Limam, A.** and **Berthet-Rambaud, P.** (2008) Avalanche impact pressure on an instrumented structure. *Cold Reg. Sci. Technol.*, **54**, 206–215.

Tiefenbacher, F. and **Kern, M.A.** (2004) Experimental devices to determine snow avalanche basal friction and velocity profiles. *Cold Reg. Sci. Technol.*, **38**, 17–30.

Van Husen, D. (1987) *Die Ostalpen in den Eiszeiten*. Geologische Bundesanstalt, Vienna, 24 pp, 1 map.

Voellmy, A. (1955) Über die Zerstörungskraft von Lawinen. *Schweizerische Bauzeitung*, **73**, 159–162.

Vriend, N.M., **McElwaine, J.N.**, **Sovilla, B.**, **Keylock, C.J.**, **Ash, M.** and **Brennan, P.V.** (2013) High-resolution radar measurements of snow avalanches. *Geophys. Res. Lett.*, **40**, 1–5. doi:10.1002/grl.50134.

Ward, R.G.W. (1985) Geomorphological evidence of avalanche activity in Scotland. *Geogr. Ann.*, **67A**, 247–256.

Weber, B., **Scherr, C.**, **Bicker, F.**, **Friedl, T.** and **Büdel, B.** (2010) Respiration-induced weathering patterns of two endolithically growing lichens. *Geobiology*, **9**, 34–43.

Whitehouse, I.E. and **McSaveney, M.J.** (1983) Diachronous talus surfaces in the Southern Alps, New Zealand, and their implications to talus accumulation. *Arctic Alpine Res.*, **15**, 53–64.

Wieczorek, G. F., **Snyder, J. B.**, **Waitt, R. B.**, **Morrissey, M. M.**, **Uhrhammer, R. A.**, **Harp, E. L.**, **Norris, R. D.**, **Bursik, M. I.** and **Finewood, L. G.** (2000) Unusual July 10, 1996, rock fall at Happy Isles, Yosemite National Park, California. *Geol. Soc. Am. Bull.*, **112**, 75–85.

Wieczorek, G.F., **Stock, G.M.**, **Reichenbach, P.**, **Snyder, J.B.**, **Borchers, J.W.** and **Godt, J.W.** (2008) Investigation and hazard assessment of the 2003 and 2007 Staircase Falls rock falls, Yosemite National Park, California, USA. *Nat. Hazards Earth Syst. Sci.*, **8**, 421–432.

Zimmer, V.L., **Collins, B.D.**, **Stock, G.M.** and **Sitar, N.** (2012) Rock fall dynamics and deposition: an integrated analysis of the 2009 Ahwiyah Point rock fall, Yosemite National Park, USA. *Earth Surf. Proc. Land.*, **37**, 680–691.

Manuscript received 22 January 2013; revision 23 August 2013; revision accepted 7 October 2013